


For Reference

NOT TO BE TAKEN FROM THIS ROOM

Ex LIBRIS
UNIVERSITATIS
ALBERTAENSIS





Digitized by the Internet Archive
in 2024 with funding from
University of Alberta Library

<https://archive.org/details/Berry1973>

THE UNIVERSITY OF ALBERTA

RELEASE FORM

NAME OF AUTHOR .Richard L. Berry.....
TITLE OF THESIS .The Ageostrophic wind component over the..
 western Cordillera: Two case studies.....

DEGREE FOR WHICH THESIS WAS PRESENTED .M.Sc.....
YEAR THIS DEGREE GRANTED ..1973.....

Permission is hereby granted to THE UNIVERSITY OF
ALBERTA LIBRARY to reproduce single copies of this
thesis and to lend or sell such copies for private,
scholarly or scientific research purposes only.

The author reserves other publication rights, and
neither the thesis nor extensive extracts from it may
be printed or otherwise reproduced without the author's
written permission.

THE UNIVERSITY OF ALBERTA

THE AGEOSTROPHIC WIND COMPONENT OVER THE
WESTERN CORDILLERA: TWO CASE STUDIES

by



RICHARD L. BERRY

A THESIS

SUBMITTED TO THE FACULTY OF GRADUATE STUDIES AND RESEARCH
IN PARTIAL FULFILMENT OF THE REQUIREMENTS FOR THE DEGREE

OF MASTER OF SCIENCE

IN

METEOROLOGY

DEPARTMENT OF GEOGRAPHY

EDMONTON, ALBERTA

FALL 1973

THE UNIVERSITY OF ALBERTA

FACULTY OF GRADUATE STUDIES AND RESEARCH

The undersigned certify that they have read, and recommend to the Faculty of Graduate Studies and Research, for acceptance, a thesis entitled "The ageostrophic wind component over the Western Cordillera: Two case studies", submitted by Richard L. Berry in partial fulfilment of the requirements for the degree of Master of Science in Meteorology.

DEDICATION

To My Loving Wife, Elaine.

ABSTRACT

A method for obtaining the non-geostrophic component of the observed wind is outlined. Two techniques are used to obtain the divergence and relative vorticity of the non-geostrophic component. The effects of several influences on the ageostrophic divergence and relative vorticity are discussed, including condensational heating, gradient winds, and terrain effects.

Two case studies of the 700-400 mb layer over a portion of the Western Cordillera are presented. The results of these studies indicate that horizontal thermal advection was the dominant influence controlling the ageostrophic wind, with condensational heating and gradient wind influences having only minor effects. It is concluded that prevailing atmospheric stability and the methods of analysis employed did not permit sufficient resolution of the wind field to delineate terrain influences in the cases studied. Some suggestions for further work are made within the scope of the methods discussed which may help to determine terrain effects.

ACKNOWLEDGMENTS

It is a common turn of phrase that no man is an island, and it is with heartfelt gratitude that I mention those who helped bridge the gap between the first and last pages of this thesis.

To my supervisor, Dr. E.R. Reinelt, I express my deep appreciation for his help in preparing the manuscript, for providing several of the references, and for lending much needed moral support. I would also like to thank Dr. E.P. Lozowski and Dr. N. Rajaratnam for giving freely of their time to read the thesis and serve on the examining committee. Dennis Oracheski asked probing questions in the course of many discussions. The multilith wizardry of Mr. Jack Chesterman helped to get the diagrams into the text. The Institute of Earth and Planetary Physics paid for the microfilmed copies of the raw data.

To my wife Elaine I am particularly indebted. She helped in extracting and punching the data, and typed both the first and final drafts of the manuscript. Her patience and understanding were appreciated more than she realizes.

This work was carried out while on educational leave from the Atmospheric Environment Service of Canada.

TABLE OF CONTENTS

	Page
DEDICATION	iv
ABSTRACT	v
ACKNOWLEDGEMENTS	vi
TABLE OF CONTENTS	vii
LIST OF TABLES	x
LIST OF FIGURES	xi

CHAPTER

I	INTRODUCTORY REMARKS AND THE CALCULATION OF DIVERGENCE AND VORTICITY	1
1.1	Introduction	1
1.2	The Methods of Divergence and Vorticity Calculation	2
II	POSSIBLE SOURCES OF THE AGEOSTROPHIC WIND DEVIATIONS	5
2.1	Introduction	5
2.2	The Assumption of Incompressibility	6
2.3	Results Arising from the Gradient Wind	9
2.4	Thermally-Induced Vorticity and Divergence	12
2.5	Propagation of Errors Leading to Spurious and/or Uncertain Results	14
2.6	Divergence and Vorticity Induced in the Upper Flow by Mountainous Terrain	17
2.7	Summary	19

CHAPTER		Page
III	THE DATA AND THE ANALYSIS PROCEDURES . . .	21
3.1	The Finite-Differencing and Objective- Analysis Grid	21
3.2	Synoptic Description of Case Studies . . .	24
3.3	The Aerological and Terrain Data	26
3.4	The Objective Analysis	28
3.5	The Analysis Procedure	32
IV	THE RESULTS OF THE ANALYSES	33
4.1	Introduction	33
4.2	The Geostrophic Flow for the December Study	34
4.3	The Ageostrophic Wind Fields of the December Study	36
4.4	The Ageostrophic Divergence Fields of the December Study	38
4.5	The Ageostrophic Relative Vorticity Fields for the December Study	40
4.6	The Mean Geostrophic Flow for the January Study	43
4.7	The Mean Ageostrophic Deviations for the January Study	45
4.8	The Ageostrophic Divergence Fields of the January Study	47
4.9	The Ageostrophic Vorticity Fields of the January Study	49
4.10	Terrain and Condensational Heating Influences in the Results	51
4.11	Thermal Advection Effects for the December Study	52
4.12	Thermal Advection Effects for the January Study	53
4.13	Summary of the Results	53

CHAPTER		Page
V	SUMMARY AND CONCLUSIONS, WITH SOME SUGGESTIONS FOR FURTHER WORK	55
5.1	Summary of the Methods Employed and the Calculated Results	55
5.2	Conclusions	57
5.3	Suggestions for Further Work	57
	LIST OF SYMBOLS	60
	REFERENCES TO LITERATURE	63
APPENDIX I	DIVERGENCE AND VORTICITY USING THE BELLAMY TRIANGLE METHOD	65
APPENDIX II	GRADIENT WIND VORTICITIES AND DIVERGENCES	68
APPENDIX III	DERIVATION OF THE UNCERTAINTIES IN THE DIVERGENCE AND VORTICITIES CALCULATED BY THE FUNDAMENTAL AND BELLAMY METHODS	72
APPENDIX IV	THE EQUATIONS FOR TRANSFORMING GEOGRAPHICAL POSITIONS INTO GRID POSITIONS	79

LIST OF TABLES

Table		Page
1	A comparison of the probable error in the calculated pressure-surface heights to the observed pressure-surface heights	15
2	The probable error in the observed wind components	16
3	The uncertainties in the ageostrophic divergence and relative vorticity	18

LIST OF FIGURES

Figure		Page
1	The hypothetical field of flow for estimating the gradient wind contributions to the ageostrophic divergence and relative vorticity	11
2	The divergence and vorticity of the cyclostrophic portion of the gradient wind	12
3	The finite-difference and objective-analysis grid	23
4	The geometry for transforming the observed wind direction to be consistent with grid north . . .	24
5	The average precipitation areas for the December case study	26
6	The average precipitation areas for the January case study	27
7	The smoothed terrain of the area for which the ageostrophic winds were analyzed	30
8	The Laplacian of the smoothed terrain	30
9	The geographical area for which the ageostrophic divergence and relative vorticity were calculated	34
10	The time-averaged geostrophic flow of the December study	35
11	The time-averaged ageostrophic wind components of the December study	37
12	The ageostrophic divergence fields of the December study as calculated by the fundamental method	40
13	The ageostrophic relative vorticity fields of the December study as calculated by the fundamental method	42
14	The time-averaged geostrophic flow of the January study	44

Figure		Page
15	The time-averaged ageostrophic wind components of the January study	46
16	The ageostrophic divergence fields of the January study as calculated by the fundamental method	48
17	The ageostrophic relative vorticity fields for the January study as calculated by the fundamental method	50
A.1	The geometry of the Bellamy Triangle	66
A.2	The finite difference elements for evaluating the partial derivatives in the equations for the divergence and relative vorticity of the gradient wind	69
A.3	The grid-point ordering for calculating the geostrophic winds on a constant-pressure surface	72
A.4	The image-plane geometry for transforming latitude and longitude into grid-point positions	79

CHAPTER I

INTRODUCTORY REMARKS AND THE CALCULATION OF DIVERGENCE AND VORTICITY

1.1 Introduction

Approximations are an integral part of meteorology. Without them, most problems would be so complex as to deny solution. However, the pressure on the meteorological community to produce better forecasts covering longer periods of time has forced meteorologists to re-examine the ramifications of the approximations used in dealing with atmospheric phenomena. Interactions between the Earth's surface and the atmosphere have emerged as one of the major areas where rough approximations are no longer sufficient. In particular the Western Cordillera is a factor which must be given due consideration: it affects atmospheric motions on all scales -- from the valley wind to the planetary wave. The advent of the digital computer and the profusion of numerical circulation models which followed, have done much to clarify the mountain-atmosphere interaction. This clarification (for synoptic scale features) has come about principally through the use of the ω -equation in conjunction with the quasi-geostrophic equations (cf. Haltiner, 1971). As Sawyer (1959) points out, the quasi-geostrophic system does not permit the evaluation of ageostrophic effects since this type of motion is ignored by the equations. While this does not appear to be a serious defect for broad (~ 1000 km.) and low (maximum height ~ 300 m) mountains, ageostrophic effects arising from a barrier having the dimensions and complexity of the Western Cordillera may be significant.

On the synoptic scale, terrain-induced vertical motions have an important influence on developments in the vicinity of mountains. Since these induced vertical velocities must eventually be damped out at some level above the terrain, it follows that they must create a localized field of horizontal divergence and convergence. Namias and Clapp (1946) discovered this field while using monthly mean maps of the 10,000 foot level (~ 700 mb). They remarked on its seasonal consistency and attributed it to topographical effects. To the extent that the ageostrophic wind is neglected in the quasi-geostrophic numerical

formulations, it follows that the divergence and relative vorticity of this component will also be neglected. It is the intended purpose of this study to try and determine if the ageostrophic wind component over the Western Cordillera shows any evidence on a synoptic scale of spatial organization that can be attributed to terrain influence in terms of divergence and the vertical component of the relative vorticity.

The data-gathering network around and in the Cordillera is not sufficiently dense to permit an investigation at any level below that of the highest level of the terrain i.e. ~ 3000 m in the region studied. The 700 mb level was chosen as the lowest acceptable level to be examined. Induced vertical motions will be the principal agent by which terrain effects are communicated to the upper levels of the atmosphere. At the 400 mb level these velocities will generally be about one order of magnitude less than their initial value (Berkofsky, 1964), hence the analysis was terminated at this level.

The methods employed will be simple in view of the lack of an adequate theory dealing with ageostrophic winds. The ageostrophic components will be found by subtracting an objectively-analyzed geostrophic wind from the observed wind vectors. The calculation of the divergence and vertical component of relative vorticity is discussed in section 1.2. Later discussion (section 2.5) will show the limited accuracy of these methods, with the result that the presence, and not the magnitude, of ageostrophic effects will be of prime concern.

It should be noted at this point that the (x, y, p, t) coordinate system will be used throughout this thesis. The coordinates x and y will refer to the finite difference grid in the normal Cartesian sense. In this respect $u = dx/dt$, and $v = dy/dt$. All motions will be with reference to a constant pressure surface, and subscript "A" will denote ageostrophic.

1.2 The Methods of Divergence and Vorticity Calculation

To obtain consistent and reasonable estimates of atmospheric vorticity and divergence is a continuing problem in synoptic meteorology. Numerous techniques have been proposed and used for computing these quantities. The method chosen depends on many factors,

some of which are:

- The purpose for which the quantities are being obtained;
- The required accuracy;
- The quality and amount of initial data required or available;
- The ease of computation;
- The atmospheric processes to be taken into consideration.

Deciding on the method to be used usually involves a compromise of one or more of these factors. Two methods appropriate for the ageostrophic winds were chosen for use in this study. The first method will be called the Fundamental Method in which

$$D_F = \left(\frac{\partial u}{\partial x} + \frac{\partial v}{\partial y} \right)_p \quad (1.2.1)$$

$$Q_F = \left(\frac{\partial v}{\partial x} - \frac{\partial u}{\partial y} \right)_p$$

where D_F and Q_F are respectively the horizontal divergence and vertical component of relative vorticity in the (x,y,p,t) coordinate system. The principal advantage in using (1.2.1) lies in the ease with which these equations can be evaluated. However, the fundamental method has an inherent disadvantage which must be recognized when it is used. This drawback is its sensitivity to errors and Gaussian noise in the initial observations, and in subsequent analyses of both the pressure-surface heights and the wind vector. Observational errors can be partially removed by careful checking, but Gaussian noise is difficult to remove because of the rather arbitrary nature of the choice as to what constitutes noise. While methods of polynomial fitting and harmonic analysis have been devised for minimizing the above mentioned errors, their usage is again limited by what is chosen as the level of significance.

As a compromise, the decision was made to use the time-averaged ageostrophic components as the basis for calculating the divergence and vorticity by the use of (1.2.1) under the assumption that the actual uncertainties in the values for specific times would tend to cancel in the averaging procedure, even though the theoretical uncertainty is increased (section 2.5). The averaging may also remove

or minimize unwanted ageostrophic effects accompanying minor disturbances moving through the region studied. The shifting of the flow patterns during the interval over which the averages were taken will mean that the calculated results will apply to the mean flow of the period.

The second method of estimating the vorticity and divergence of the ageostrophic deviation is that proposed by Bellamy (1949). If it can be assumed that variations in the wind field are linear between any two observing stations forming the vertices of a triangle, then it can be shown (Appendix I) that the divergence and relative vorticity of the flow contained within the triangle are given by:

$$\begin{aligned} D_B &= \sum_{i=1}^3 -\frac{V_{A_i}}{h_i} \sin(\beta_i - \alpha_i) \\ Q_B &= \sum_{i=1}^3 \frac{V_{A_i}}{h_i} \cos(\beta_i - \alpha_i) \end{aligned} \quad (1.2.2)$$

in which subscript i represents the i^{th} vertex of the triangle, V_A is the ageostrophic wind speed, β_i is the azimuth of the opposing side and α_i is the direction of V_A (both measured clockwise from the positive y axis of the grid), and h_i is the length of the perpendicular to the opposing side through the i^{th} vertex.

As employed in this study, the Bellamy method requires several considerations. First, since it was used on the ageostrophic wind field, it will be sensitive to the accuracy of the observed winds and pressure-surface heights. Second, the triangles employed should be as close to being equilateral as possible. This is necessary to ensure that the results represent two-dimensional phenomena. To satisfy this condition, no triangle should have any interior angles greater than 90° .

The third factor to consider is the point in space to which the Bellamy estimates apply. If the triangles were perfectly equilateral, the obvious choice would be the point at which the bisectors of the interior angles intersect. The triangles used in this study were not truly equilateral, with the result that the "center of gravity" of the triangle was chosen as the point to which

the results would apply. Eddy (1973) indicates that this will introduce a geometrical bias into the results.

The assumption of linear variations in the ageostrophic wind field between stations appears reasonable with the scale of analysis used and the size of the variations involved.

CHAPTER II

POSSIBLE SOURCES OF THE AGEOSTROPHIC WIND DEVIATIONS

2.1 Introduction

To obtain the ageostrophic deviation, the wind field was decomposed into two components -- one in geostrophic balance (\vec{V}_g), and a non-geostrophic component (\vec{V}_A). Hence, the observed wind (\vec{V}) can be represented mathematically as:

$$\vec{V} = \vec{V}_g + \vec{V}_A \quad (2.1.1)$$

Thus, from (2.1.1) we have:

$$\begin{aligned} u_A &= u - u_g \\ v_A &= v - v_g \end{aligned} \quad (2.1.2)$$

where

$$\begin{aligned} u_g &= -\frac{g}{f} \left(\frac{\partial Z}{\partial y} \right)_p \\ v_g &= \frac{g}{f} \left(\frac{\partial Z}{\partial x} \right)_p \end{aligned} \quad (2.1.3)$$

in which Z is the geopotential height of the reference surface p , the acceleration due to gravity is g , and f represents the Coriolis parameter.

To presuppose that the ageostrophic deviations calculated are generated solely by terrain influences would be folly since ageostrophic deviations may arise from many factors. However, to try and decompose them into components due to each, while theoretically possible in some cases, would be very difficult for practical purposes. In lieu of this, the rest of this chapter will be devoted to discussing the effects that the influences listed below would have on the values of divergence and vorticity of the ageostrophic wind, to aid in

interpreting the results:

- (i) Atmospheric compressibility,
- (ii) The presence of curved flow (i.e. the "gradient wind")
- (iii) Thermal influences due to condensation processes,
- (iv) Propagation of measurement errors,
- (v) Terrain influences.

2.2 The Assumption of Incompressibility

Batchelor (1967) employed the methods of scale analysis to the study of the conditions under which the assumption of incompressibility was justified when considering the velocity distribution in a moving fluid. He assumed that the fluid flow can be characterized by a scale length L such that variations in the fluid velocity \vec{v} are small over distances that are small compared with L . Furthermore, the variations of \vec{v} in both time and space are assumed to have the magnitude U . The order of magnitude of the spatial derivatives of components of \vec{v} will then be given by U/L . For the purposes of this study, the length scale was chosen to be half the width of the main current at 500 mb which was found to be about seven degrees of latitude, or roughly 8×10^5 meters at 45°N . The scale velocity thus becomes the central value of this current which has a typical value of about 40 m sec^{-1} .

Let us assume an atmosphere having constant composition and choose as the parameters of state the density ρ and specific entropy S . Then the rate of change of pressure experienced by a material element can be expressed as:

$$\frac{dp}{dt} = c^2 \frac{d\rho}{dt} + \left(\frac{\partial p}{\partial S} \right)_\rho \frac{dS}{dt} \quad (2.2.1)$$

Rearranging (2.2.1) gives:

$$\frac{1}{\rho} \frac{d\rho}{dt} = \frac{1}{\rho c^2} \frac{dp}{dt} - \frac{1}{\rho c^2} \left(\frac{\partial p}{\partial s} \right)_p \frac{ds}{dt} \quad (2.2.2)$$

But

$$-\frac{1}{\rho} \frac{d\rho}{dt} = \nabla \cdot \vec{V}$$

and it is to be shown that

$$|\nabla \cdot \vec{V}| \ll U/L$$

Hence the assumption of incompressibility will be justified if:

$$\left| \frac{1}{\rho c^2} \frac{dp}{dt} - \frac{1}{\rho c^2} \left(\frac{\partial p}{\partial s} \right)_p \frac{ds}{dt} \right| \ll \frac{U}{L} \quad (2.2.3)$$

At this point the mathematics becomes somewhat involved. The total derivatives in (2.2.3) are expanded (using the isentropic assumption to expand dp/dt) and the condition is imposed that all terms must be much less than U/L . The reader is referred to Batchelor's text for the details, but the resulting inequalities are given by:

- (i) $\frac{U^2}{c^2} \ll 1$
- (ii) $\frac{n^2 L^2}{c^2} \ll 1$
- (iii) $\left| \frac{W}{U} \right| g \frac{L'}{c^2} \ll 1$
- (iv) $\frac{\beta' U^2}{c_p} \frac{\mu}{\rho L U} \ll 1$
- (v) $\beta' \theta \frac{\kappa}{L U} \ll 1$

in which:

$\kappa' =$ A measure of the dominant frequency of oscillation in the flow field, chosen to be every three days or about $4 \times 10^{-6} \text{ sec}^{-1}$

$\beta' =$ The isobaric coefficient of thermal expansion
 $= 3.92 \times 10^{-3} \text{ }^\circ\text{C}^{-1} @ -17.8^\circ\text{C and 1013 mb}$

$C_p =$ Specific heat at constant pressure of dry air
 $= 0.240 \text{ cal. gm}^{-1} \text{ }^\circ\text{C}^{-1}$

$\frac{\mu}{\rho} = \nu$ the kinematic viscosity
 $= 0.132 \text{ cm}^2 \text{ sec}^{-1} @ 0^\circ\text{C and 1013 mb}$

$\theta =$ A measure of the temperature differences in the fluid, chosen to be 50°C

$\kappa =$ The thermal diffusivity of dry air
 $= 0.184 \text{ cm}^2 \text{ sec}^{-1} @ 0^\circ\text{C}$

$C =$ The local adiabatic speed of sound
 $\cong 320 \text{ m sec}^{-1} @ 5 \text{ km}$

$L' =$ The scale of vertical motions, chosen to be the height of a homogenous ($\rho = \text{constant}$) atmosphere or is approximately $8 \times 10^3 \text{ m}$

$W =$ Magnitude of vertical velocities, chosen to be approximately 0.1 m sec^{-1}

Substitution into the inequalities (i)-(v) shows that all left-hand sides are at least two orders of magnitude less than unity. This was considered sufficient to warrant neglecting atmospheric compressibility, and hence its contribution to the divergence or vorticity of the ageostrophic wind.

2.3 Results Arising from the Gradient Wind

The flow patterns of the atmosphere, in the cases chosen for study, show evidence that in some areas the consideration of a gradient wind would be appropriate. Unfortunately, the necessity of calculating the curvature of the flow makes the gradient wind a difficult quantity to calculate with any degree of accuracy.

The definition of a streamline may be expressed as:

$$\frac{dy}{dx} = \frac{v}{u} \quad (2.3.1)$$

where y is a function of x only. If we assume that the observed wind speed (V) is in fact the gradient wind speed G , then:

$$u^2 + v^2 = G^2 \quad (2.3.2)$$

Let us further assume that the flow can be represented by an infinitely broad current flowing from west to east in which the equation of a streamline is given by:

$$y_i = a e^{-\frac{x^2}{\lambda}} + i\Delta \quad (2.3.3)$$

where a, λ and Δ are constants and Δ can be any desired contour spacing. A Value of $a=1$ and $\lambda =20$ was found to yield a contour shape shwon in Figure 1 which is roughly similar to those of interest in the case studies if x and y are in units of grid-interval.

Petterssen¹ also gives the following expressions for the vorticity (Q) and divergence (D) of the wind along a streamline:

$$D = \frac{\partial V}{\partial s} + V \frac{\partial \beta}{\partial n} \quad (2.3.4)$$

$$Q = VK_s - \frac{\partial V}{\partial n}$$

where β is the angle which the wind makes with the x axis, K_s is the curvature of the streamline, and s and n measure distance along and perpendicular to the left of the streamline if moving in the direction of the flow. For the purposes of this analysis, the streamlines, trajectories, and contours will be assumed to be coincident and given by (2.3.3).

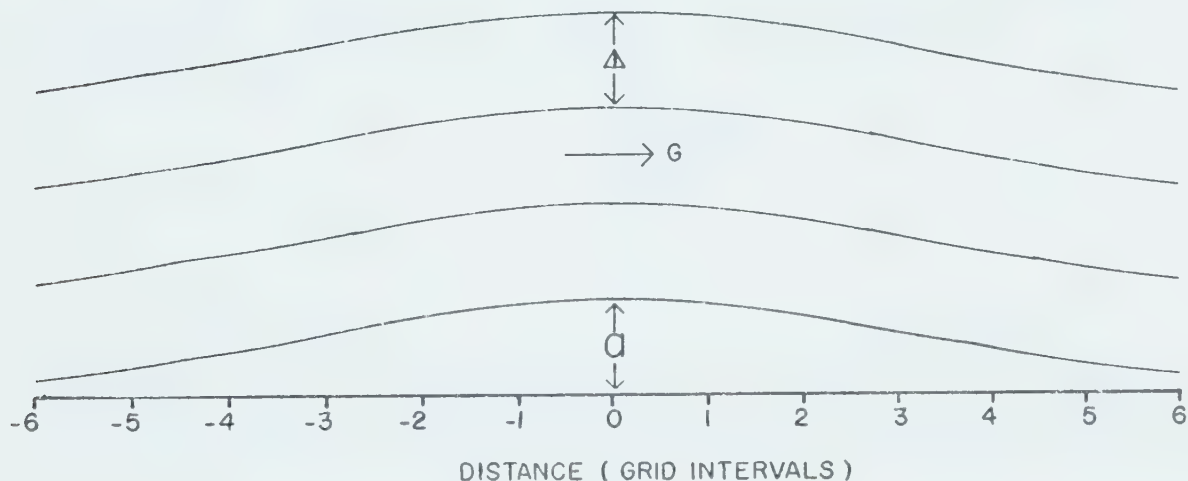


Fig. 1 The hypothetical field of flow for estimating the gradient wind contribution to the ageostrophic divergence and relative vorticity.

¹ See Petterssen (1956) page 42.

Substitution into (2.3.4) gives:

$$D_G = \frac{\partial G}{\partial s} + G \frac{\partial \beta}{\partial n} \quad (2.3.5)$$

$$Q_G = \frac{G}{R} - \frac{\partial G}{\partial n}$$

where the substitution $K_s = 1/R$ has been made, R being the radius of curvature of the contour. Subscript G denotes "of the gradient wind".

The final assumption to be made is that the gradient wind speed (G) involved in the equations (2.3.5) is the maximum possible at any point along the contour. Making this assumption, and setting G to some constant value such that it will not be a function of position, will lead to calculated results which are the maximum possible at any given point along the contour for the chosen gradient wind speed.

Using these assumptions, equations (2.3.5) were evaluated (see Appendix I) for the flow pattern of Figure 1, assuming a value for G of 40 m sec^{-1} ; the results are shown in Figure 2.

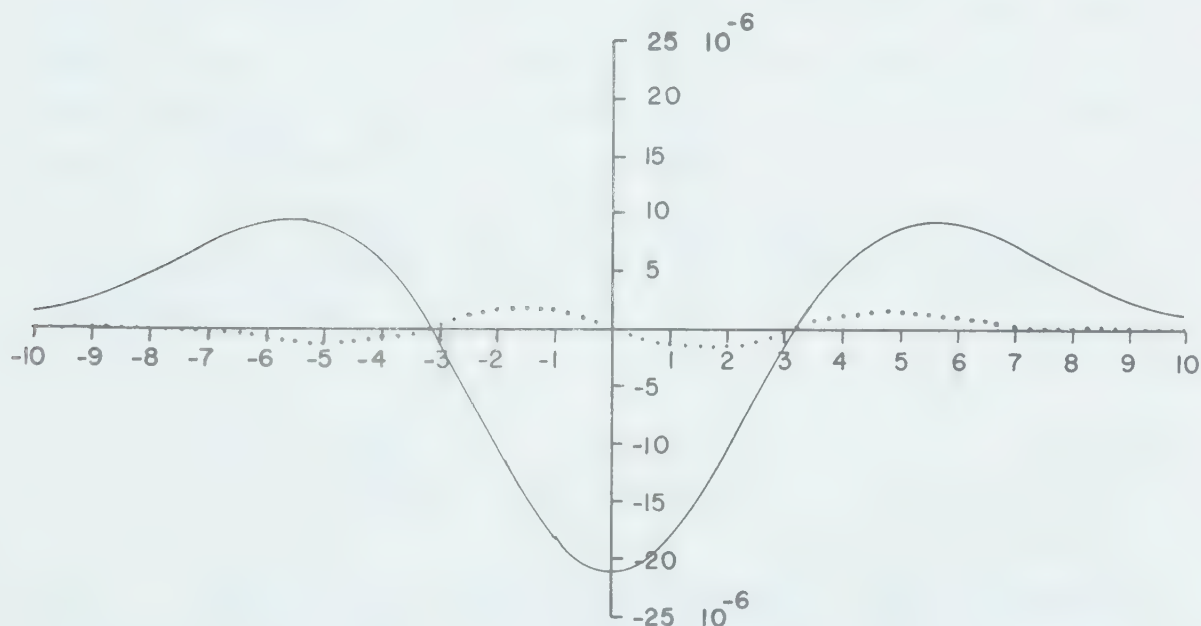


Fig. 2 The divergence (dotted line) and vorticity (solid line) of the gradient wind for the flow field of Fig. 1 using $G=40 \text{ m sec}^{-1}$. Ordinate units are sec^{-1} , abscissa units are taken to be grid intervals

An examination of these results indicates that the relative vorticity of the gradient wind may be of the order of 10^{-5} sec^{-1} for strong flow exhibiting moderate curvature. The divergence arising from this wind does not appear to be significant, having a maximum value of order 10^{-6} sec^{-1} . For values of G other than 40 m sec^{-1} , for instance G' , the relationships:

$$\begin{aligned} D_{G'} &= \left(\frac{G'}{40} \right) D_{40} \\ Q_{G'} &= \left(\frac{G'}{40} \right) Q_{40} \end{aligned} \tag{2.3.6}$$

can be employed using the results in Figure 2.

2.4 Thermally Induced Vorticity and Divergence

Danard (1964) in a case study of a rapidly developing cyclone found that the release of latent heat due to condensation in the free atmosphere could result in considerable changes in the large-scale vertical motions. Vertical velocities in areas of active condensation were found to vary by a factor of two or three from those calculated when release of latent heat was neglected. In a previous but similar study by Aubert (1957), the same conclusions were drawn, and it was shown that these effects are rapidly damped as one moves away from the region in which condensation is occurring.

These two studies indicate that a consideration of thermal effects can considerably alter the derived patterns and magnitudes of vertical velocity. Thus, since:

$$D_p = - \frac{\partial \omega}{\partial p} \tag{2.4.1}$$

where D_p represents the isobaric divergence on a constant pressure surface and $\omega = dp/dt$, it is evident that an inclusion of thermal effects may alter the magnitudes and distributions of divergence and vorticity along a constant-pressure surface.

Let us assume that the wind speed at a point in the free atmosphere, with no condensation occurring, is given by:

$$\vec{V}_T = \vec{V}_0 + w_0 \hat{k} \quad (2.4.2)$$

Let us further assume that if condensation occurred at this point, then the vertical speed would be doubled, while the total wind (\vec{V}_T) remained the same such that:

$$\vec{V}_T = \vec{V}_c + 2w_0 \hat{k} \quad (2.4.3)$$

where \vec{V}_c represents the wind components along the pressure surface with condensation. Solving (2.4.2) and (2.4.3) for the change in horizontal wind speed gives:

$$\vec{V}_D = w_0 \hat{k}$$

where

$$\vec{V}_D = \vec{V}_c - \vec{V}_0$$

Thus, in order for the horizontal wind to change by only one meter per second, the initial vertical wind speed would have to be at least one meter per second. Vertical velocities of this magnitude generally occur only in the most intense subsynoptic systems. A more likely vertical velocity of say 10 cm sec^{-1} would require an adjustment of only 0.1 m sec^{-1} in the horizontal components. Resolution of the wind vector to this degree with the data available is not possible.

In view of this, quantitative estimates of the effects of condensational heating were considered impractical with the methods of calculation employed. However, qualitative judgments were made if such were considered necessary.

2.5 Propagation of Errors Leading to Spurious and/or Uncertain Results

In as much as this study is basically an analysis of atmospheric measurements, it was deemed necessary to examine how the errors in these measurements would affect the calculated values of divergence and vorticity. The method of error analysis chosen was that outlined by Baird (1962).

As part of the data check, the heights of the 700, 600, 500, and 400 mb surfaces computed using the hydrostatic assumption were compared to the values reported on the ascent recordings. If the observed heights are accepted as the correct values, then the probable error (P.E.) in the calculated values would be given by:

$$P.E. = \frac{2}{3} \sqrt{\sigma_D^2} \quad (2.5.1)$$

where σ_D^2 represents the variance of the difference in the two height values.

However, the observed height values are not the "true" values, but incorporate errors from several sources, such as instrument and observer errors. An estimate of the observational errors was obtained from a study done by Rapp (1952). The probable error calculated by the method given above, and Rapp's estimates of the error in the observed heights are given in Table 1.

Pressure Level (mb)	P. E. _{CH} (gpm)	P. E. _{OH} (gpm)
700	± 2.1	± 4.7
600	2.1	5.8
500	2.4	6.8
400	2.7	11.7

Table 1. A comparison of the probable error in the calculated heights accepting the observed value as correct (P.E. _{CH}) and the probable error in the observed heights (P.E. _{OH}).

Since the difference between the calculated and observed heights lies well within observational error, it was decided that the observational errors given by Rapp could be used as the uncertainty in the calculated heights (δZ) of the various pressure surfaces.

The uncertainty in the heights of the pressure surfaces will lead to an uncertainty in the calculated geostrophic winds as defined by (2.1.3), which in turn will lead to further uncertainty in the ageostrophic components defined by (2.1.2). Note that there will also be a contribution to the error in the ageostrophic components due to uncertainties in the observed wind speeds ($\delta u, \delta v$). Rapp's values for the probable error in the observed wind speeds are given in Table 2.

Height (km)	P.E. u (m sec ⁻¹)	P.E. v (m sec ⁻¹)
0.5	0.21	0.35
1.0	0.45	0.45
1.5	0.38	0.27
2.0	0.42	0.18
2.5	0.51	0.53
3.0	0.43	0.41
3.5	0.24	0.19
4.0	0.31	0.60
4.5	0.46	0.65
5.0	0.83	0.99
5.5	0.90	0.69
6.0	0.70	1.00
6.5	0.49	1.50
7.0	0.40	0.54
7.5	0.31	1.80
8.0	0.49	0.84
8.5	1.99	2.80

Table 2. The probable error in the observed wind components (after Rapp, 1952).

Rapp attributes the inconsistency in the P.E. of the wind speed between consecutive levels to the sampling technique employed. Since the errors at all levels are of the same magnitude, an arithmetic mean was used for the values from 0.5 to 7.0 km inclusive, yielding values of $\delta u = 0.48 \text{ m sec}^{-1}$ and $\delta v = 0.60 \text{ m sec}^{-1}$.

It should be noted that Rapp's error estimates are probably very conservative since the observers in the experiment and the conditions under which the raw data were collected were of a higher quality than those involved in the routine program of upper air sounding. Carrying through the error analysis as given in Appendix III gave the following expressions for the uncertainties in the divergence and vorticity as calculated by the fundamental (subscript F) and Bellamy (subscript B) methods:

$$\delta \bar{D}_F = \delta \bar{Q}_F \cong \pm \frac{2}{H} \left(\delta v + g \frac{\delta Z}{fH} \right) \quad (2.5.2)$$

$$\delta \bar{D}_B \cong \pm \frac{2}{H} \left(\frac{\bar{u}_A^2}{\sqrt{\bar{u}_A^2 + \bar{v}_A^2}} \right) \left(\delta u + g \frac{\delta Z}{fH} \right) \quad (2.5.3)$$

$$\delta \bar{Q}_B \cong \pm \frac{2}{H} \left(\frac{\bar{v}_A^2}{\sqrt{\bar{u}_A^2 + \bar{v}_A^2}} \right) \left(\delta u + g \frac{\delta Z}{fH} \right) \quad (2.5.4)$$

An examination of the ratios $\delta \bar{D}_B / \delta \bar{D}_F$ and $\delta \bar{Q}_B / \delta \bar{Q}_F$ shows that the results of the Bellamy method will generally be less uncertain than those of the fundamental method. Thus, if the two methods yield similar results, then some semblance of the actual physical situation can be attributed to the calculated values in spite of the large potential for error shown by the sample results of Table 3.

Level (mb)	$\oint D_F, \oint Q_F$ (sec ⁻¹)
700	$\pm 31 \times 10^{-6}$
600	37
500	42
400	67

Table 3. The uncertainties in the ageostrophic divergence and vorticity given by (2.5.2) using $H=185.3$ km, $\oint v=0.60$ m sec⁻¹, $f=1.1 \times 10^{-4}$ sec⁻¹ at 50°N, and Table 1.

2.6 Divergence and Vorticity Induced in the Upper Flow by Mountainous Terrain

If an air stream impinges on a mountain barrier, the terrain-induced vertical motions will have an effect on the air stream. Berkofsky (1964) studied three methods of computing the fall-off with height of the terrain-induced vertical motions. He suggested that equation (2.6.3) is a viable alternative to more complicated methods.

$$\frac{\omega}{\omega_{p_0}} = \left(\frac{p}{p_0} \right)^{\kappa} \left(\frac{\xi_{p_0}}{\xi} \right) \quad (2.6.3)$$

Where ω_{p_0} is the vertical velocity at the initial level p_0 and:

$$\xi = \frac{\partial T}{\partial p} - \kappa \frac{T}{p}$$

is the stability factor with:

$$\kappa = \frac{R}{c_p} = 0.288$$

Studies by Charette (1971) and Hopkinson (1972) suggest that terrain induced vertical motions over the Western Cordillera can be of the order of ± 10 -20 cm sec⁻¹ (or roughly ± 10 -20 μ b sec⁻¹) at the 850-mb level. Using these figures and the radiosonde data for the case studies together with equations (2.4.1) and (2.6.3) indicated

that terrain induced divergences could be of the order of $\pm 10-30 \times 10^{-6} \text{ sec}^{-1}$ at the 625-mb level. While this is a very crude estimate, it does serve to indicate that in regions where extensive, and abrupt changes in topography occur, such as the windward and the lee slopes of the Western Cordillera, the resulting vertical motions may generate divergence at levels well above the terrain that is synoptically significant if the motions are sustained over a large enough area.

No suitable method could be found for estimating terrain induced vorticities in a simple fashion. Clearly, the largest terrain effects must occur at the point at which the atmosphere and the surface are in contact (i.e. the boundary layer). If one assumes that the terrain itself is a pressure surface such that variations in the height Z of the pressure surface are given by variations in the height of the terrain, then the expression for the relative vorticity Q of this hypothetical surface assuming the Coriolis parameter f does not vary would be given by:

$$Q = \frac{g}{f} \nabla_p^2 Z \quad (2.6.4)$$

The values of Q so produced are of the order of 10^{-3} sec^{-1} assuming a grid interval of 185.3 km in the area of interest (see Section 3.1). While the processes of atmospheric dissipation rapidly reduce this value, some portion must be transferred to higher levels of the atmosphere by vertical motions. However, the nature of the decay is not certain; hence the portion of the calculated ageostrophic vorticity arising from terrain effects must also be uncertain. In view of these problems, the calculated relative vorticities will be compared with the terrain Laplacian for agreement in sign, with due allowance given to the other factors discussed in this chapter.

2.7 Summary

- (i) Having shown in Section 2.2 that the assumption of incompressibility is justified for the scales of motion involved in this study, divergence and vorticity arising from compressibility effects were considered undetectable, and therefore neglected.
- (ii) The contribution to the ageostrophic wind from condensational heating is felt to be undetectable with the quality of the data available. However, the effects on the magnitude of the calculated divergence may be significant and will be acknowledged in a qualitative manner.
- (iii) The flow patterns indicate that the cyclostrophic component of the gradient wind may contribute significantly to the ageostrophic wind. In areas where this occurs, allowance was made in the calculated divergence and vorticity by using the results in Figure 2 and (2.3.6).
- (iv) Propagation of observational errors through the calculations leads to large uncertainties in the divergence and vorticity. A rough estimate shows that the values calculated by the Bellamy method will generally be less uncertain than those of the fundamental method. In interpreting the calculated fields-of divergence and vorticity, more emphasis will be placed on those regions where the results of the two methods are comparable.
- (v) Terrain induced vertical velocities may make a significant contribution to the field of horizontal velocity divergence. The magnitude of this contribution will depend on the speed and direction of the low level flow (i.e. below 700 mb) since this will affect the initial vertical velocities. However, a rough estimate indicates that terrain induced divergence of the order of $10\text{-}30 \times 10^{-6} \text{ sec}^{-1}$ may exist. The terrain contributions

to the ageostrophic vorticity patterns at and above 700 mb are questionable, hence the patterns will only be compared with the terrain Laplacian for qualitative correlation.

CHAPTER III

THE DATA AND THE ANALYSIS PROCEDURES

3.1 The Finite-Differencing and Objective-Analysis Grid

The grid employed was designed to be used in conjunction with a polar-stereographic map projection having a standard latitude of 60°N. The grid interval H used is 185.3 km. The reference meridian chosen is 80°W since it is roughly parallel to the Alberta portion of the Rocky Mountains and facilitates the interpretation of the results. An initial grid of 14x10 grid intervals was used giving 165 grid points. As shown in Figure 3 the geographical area covered includes Washington, Oregon, Idaho, and most of British Columbia, Alberta, Wyoming, Montana, and Nevada. The radiosonde stations used for the raw data are shown in Figure 3.

The equations for finding the grid coordinates of the data points from their latitude and longitude are derived in Appendix IV. The pertinent two relations are:

$$y_s = 15 + \frac{J}{H} \left(\tan \frac{\psi_p}{2} \cos \alpha_p - \tan \frac{\psi_s}{2} \cos \alpha_s \right) \quad (3.1.1)$$

$$x_s = 1 + \frac{J}{H} \left(\tan \frac{\psi_s}{2} \sin \alpha_s - \tan \frac{\psi_p}{2} \sin \alpha_p \right) \quad (3.1.2)$$

in which subscripts p and s represent "principal-grid-point" and "station" respectively, ψ is the co-latitude, $\alpha_{s,p}$ is the angle between the reference meridian (80°W) and the meridian through the point, $J = R_E(1 + \cos \psi_0)$ where R_E is the radius of the earth and ψ_0 is the standard co-latitude.

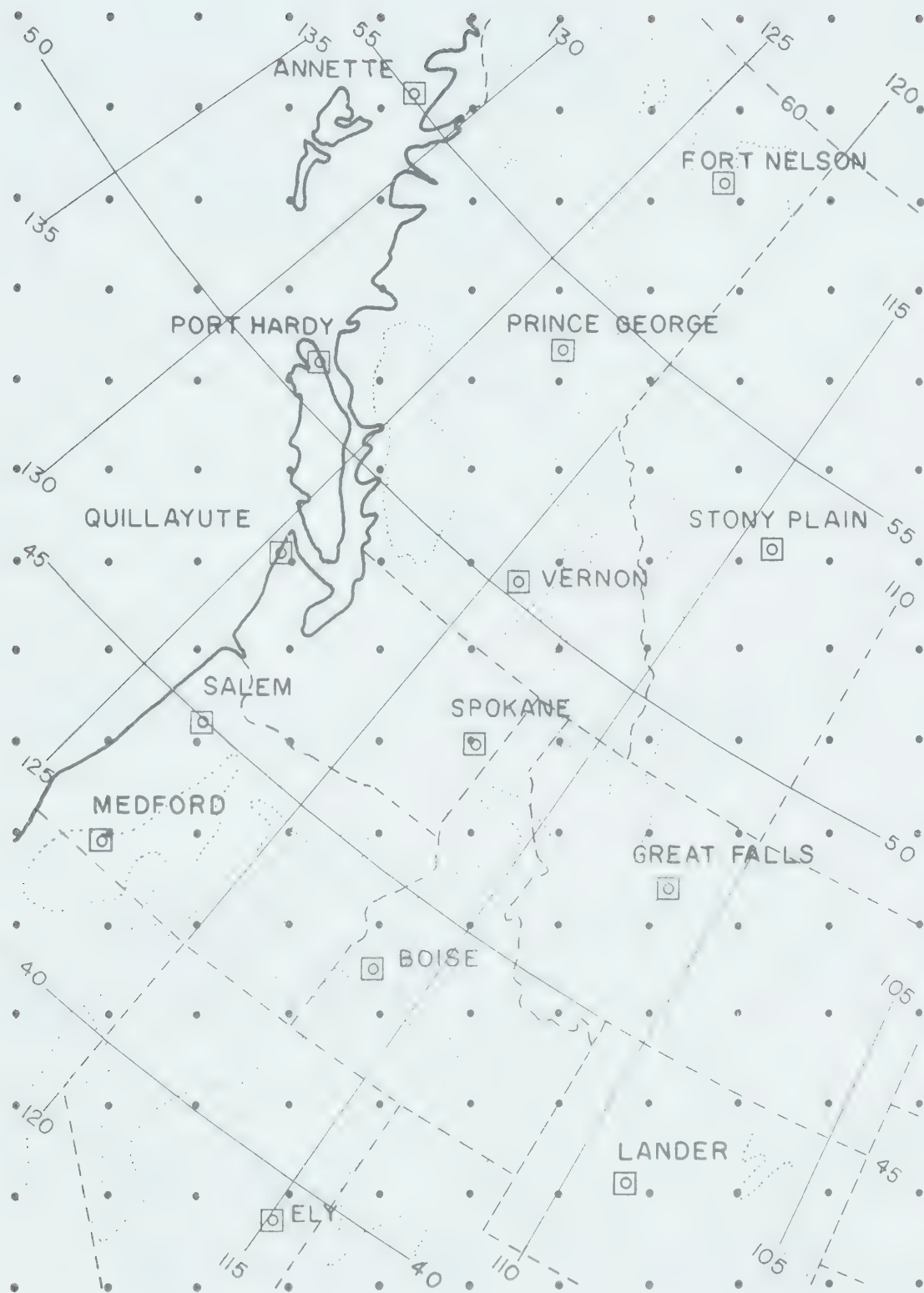


Fig. 3 The finite-difference and objective-analysis grid. Stations shown are the data points. The thin dotted line is the approximate position of the 1500 m ASL terrain contour. Grid interval is 185.3 km.

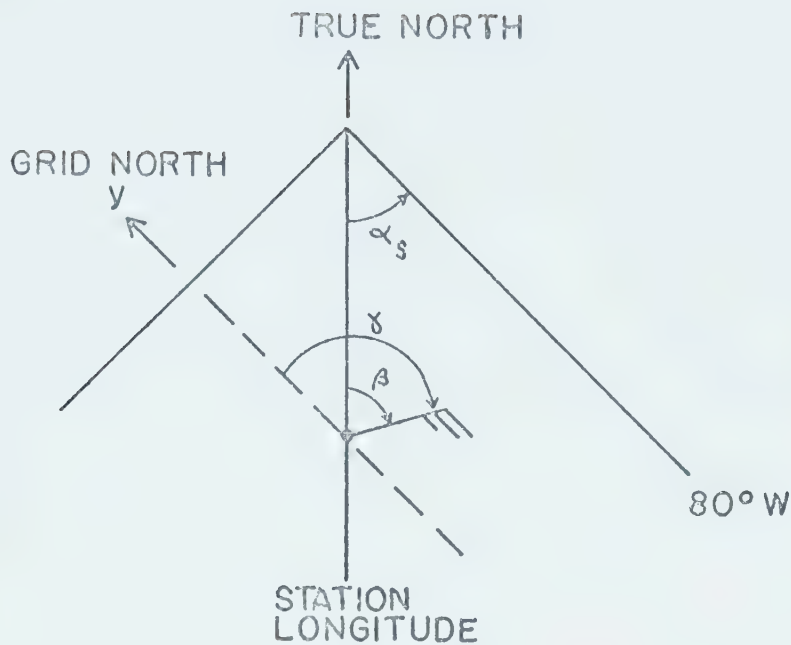


Fig. 4 The geometry for transforming the observed wind direction to yield wind components which are referred to grid north.

The observed wind direction must be transformed in order to obtain component velocities which are consistent with the grid employed. Using the geometry shown in Figure 4, the transformed wind components are given by equations (3.1.3)

$$u = -V \sin \gamma \quad (3.1.3)$$

$$v = -V \cos \gamma$$

$$\text{where } \gamma = \beta - \alpha_s - 360 \quad \text{if } \beta - \alpha_s > 360$$

$$\gamma = 0 \quad \text{if } \beta - \alpha_s = 360$$

$$\gamma = \beta - \alpha_s \quad \text{if } 0 \leq \beta - \alpha_s < 360$$

and β is the wind direction measured clockwise from true north.

3.2 Synoptic Description of Case Studies

Two cases were chosen for this study. The first case covered the period from 21 December 1200 GMT to 24 December 0000 GMT 1971, inclusive. The upper-level flow during this period was dominated by a strong low in the Gulf of Alaska which moved rapidly out of the Gulf at the end of the period to a position about 300 nautical miles west of the Oregon coast. A weak quasi-stationary ridge from Central Alberta to the Dakotas persisted through the period and maintained a strong to moderate flow from the southwest over southern British Columbia and Washington State. Dewpoint depressions over the area at 700 mb were in the 0-5°C range for most of the period.

The surface charts showed a double-centered low pressure system, with one center near Queen Charlotte Island, and the other about 100 nautical miles southwest of Vancouver Island. This system was bringing maritime air into southern British Columbia and Alberta as well as the Pacific Northwest states. An Arctic high was over Alaska and pushing continental Arctic air into Alberta from the northeast. During the period the Arctic high broke down, but an unstructured region of high pressure was set up over Alberta and Saskatchewan. The low centers combined and shifted slightly south to join with a low which moved up the United States coast. The baroclinic zone shifted from southern British Columbia and Alberta into the Washington, Idaho, and Montana area.

The second case studied in detail covered the period 16 January 1200 GMT to 18 January 0000 GMT, 1972 inclusive. The synoptic features were similar to the previous case. At the beginning of the period the upper flow was characterized by a strong low over the Gulf of Alaska with a trough extending into northeastern Saskatchewan. During the period the upper low weakened into a broad trough on a NNE-SSW line through northwestern British Columbia. A weak ridge from Edmonton to Great Falls, Montana, persisted through most of the period. The major current shifted south from central British Columbia and Alberta to a position near the United States border, maintaining a rough east-west orientation throughout the period. Dewpoint depressions at 700 mb were in the 0-5°C range over most of the region for most of the period.

Surface features were marked by a strong low in the Gulf of Alaska bringing maritime air into southern British Columbia and Alberta. During this period an Arctic high moved into northern Alaska and stalled there, pushing continental Arctic air into Alberta, and driving the baroclinic zone south through Central British Columbia and Alberta. By the end of the period the Gulf low had weakened considerably, but exhibited only a minor southward shift, while the baroclinic zone extended through southern British Columbia and Alberta

In both cases studied, there was considerable cyclonic activity along the baroclinic zone although no major developments ensued. The regions over which continuous precipitation occurred during the periods was analyzed and an average precipitation area produced for each case as shown in Figures 5 and 6.

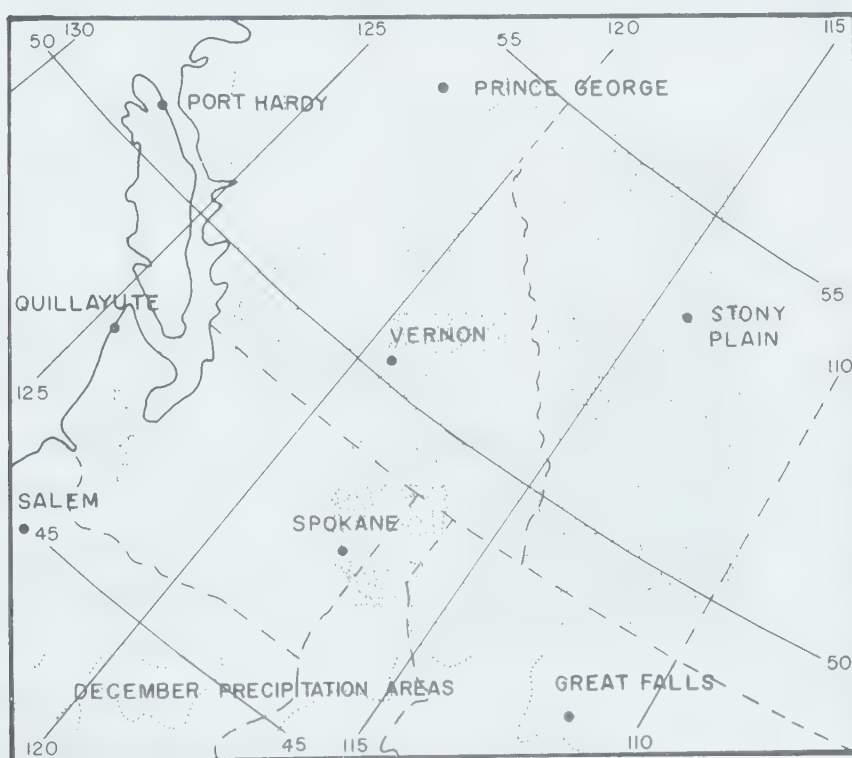


Fig. 5 The average areas where precipitation occurred during the period 21 December 1200 GMT to 24 December 0000 GMT, 1971, over that portion of the grid where the ageostrophic winds were analyzed.

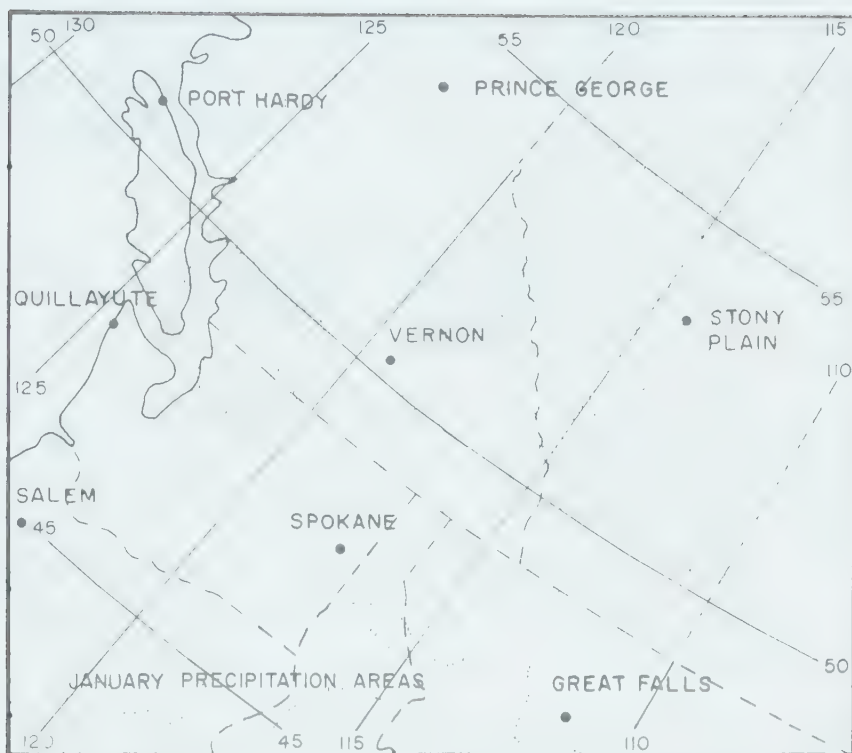


Fig. 6 Same as Fig. 5 except for the period 16 January 1200 GMT to 18 January 0000 GMT, 1972.

3.3 The Aerological and Terrain Data

Since analyses were desired at levels not reported in the monthly summaries of radiosonde ascents, it was necessary to obtain the records of complete upper-air soundings. Data for Canadian radiosonde stations were available from the Atmospheric Environment service as Adiabatic Charts and Winds Aloft Computation forms. Data for United States stations came from the U.S. Department of Commerce Environmental Data Service as WBAN 31 Adiabatic Charts, WBAN 20 Winds Aloft Computation Sheets and RAOB Computer listings. All data were obtained on microfilm.

Pressure, temperature, relative humidity (or dewpoint depression), wind speed, and wind direction were abstracted onto coding sheets from the above sources at all reported levels up to

and including the 200 mb level where possible. The abstracted data were then transferred onto punch cards for computer analysis. The height in geopotential meters Z of the desired levels was obtained using the standard equation:

$$Z_{i+1} = Z_i - \frac{R \bar{T}^*}{9.8} \ln \left(\frac{P_{i+1}}{P_i} \right) \quad (3.3.1)$$

in which i represents the i^{th} level, R is the gas constant for dry air, and \bar{T}^* is the mean virtual temperature in Kelvin degrees of the layer between pressures P_i and P_{i+1} . At pressure levels where the temperature and moisture variables were not specifically given, they were obtained by linear interpolation between the reported values above and below that of the desired level. The interpolated values were used in (3.3.1). The calculated heights were used to obtain the wind speed and direction at the desired levels from the wind sounding, by linear interpolation where necessary. Missing data were not interpolated from surrounding stations.

Several checks were made of the punched data to minimize the errors arising from the abstraction process. The punched data were checked manually against the coding sheets. The punched data were then listed by computer print-out and the print-out checked manually for apparent inconsistencies. Finally, the calculated heights of the 700, 600, 500, and 400 mb surfaces were checked against the heights reported on the adiabatic charts or RAOB computer listings. Height differences of six or more geopotential meters were considered significant for this final check.

Terrain heights were extracted at half-grid intervals over the geographical area bounded by grid points five to twelve inclusive in the y-direction, and three to eleven inclusive in the x-direction. The highest elevation within a 10 nautical mile radius of each point was used as the height at these points. To obtain the height at the full-grid points, the extracted terrain heights were averaged as

follows: for interior grid points

$$\bar{Z}_{i,j} = \frac{1}{10} \left(Z_{i-\frac{1}{2},j-\frac{1}{2}} + Z_{i,j-\frac{1}{2}} + Z_{i+\frac{1}{2},j-\frac{1}{2}} + Z_{i+\frac{1}{2},j} \right. \\ \left. + Z_{i+\frac{1}{2},j+\frac{1}{2}} + Z_{i,j+\frac{1}{2}} + Z_{i-\frac{1}{2},j+\frac{1}{2}} + Z_{i-\frac{1}{2},j} + 2Z_{i,j} \right)$$

and for grid points on the boundary

$$\bar{Z}_{i,j} = \frac{1}{3} \left(Z_{i+\frac{1}{2},j} + Z_{i,j} + Z_{i-\frac{1}{2},j} \right)$$

where $Z_{i,j}$ is the terrain height at grid point (i,j) . The Canadian terrain heights were extracted from World Aeronautical Charts ICAO, National Topographic Series (1:1,000,000). U.S. portions came from Topographic Maps of the U.S. (1:1,000,000) and National Topographic Maps (1:250,000), both published by the U.S. Department of Interior Geological Survey. The smoothed terrain contours are shown in Figure 7, and the Laplacian of the smoothed terrain is shown in Figure 8.

3.4 The Objective Analysis

The objective analysis program used was given by Glahn, Hollenbaugh and Lowry (1969). This was based on a program developed by Cressman (1959) which in turn was based on the general method described by Berghórssen and Döös (1955). It was chosen because it can analyze a height field without using the geostrophic wind relationship, although this can be included if desired (cf. Glahn and Hollenbaugh, 1969). Cressman (1959) points out that if wind is used in the analysis to obtain more accurate height gradients, then

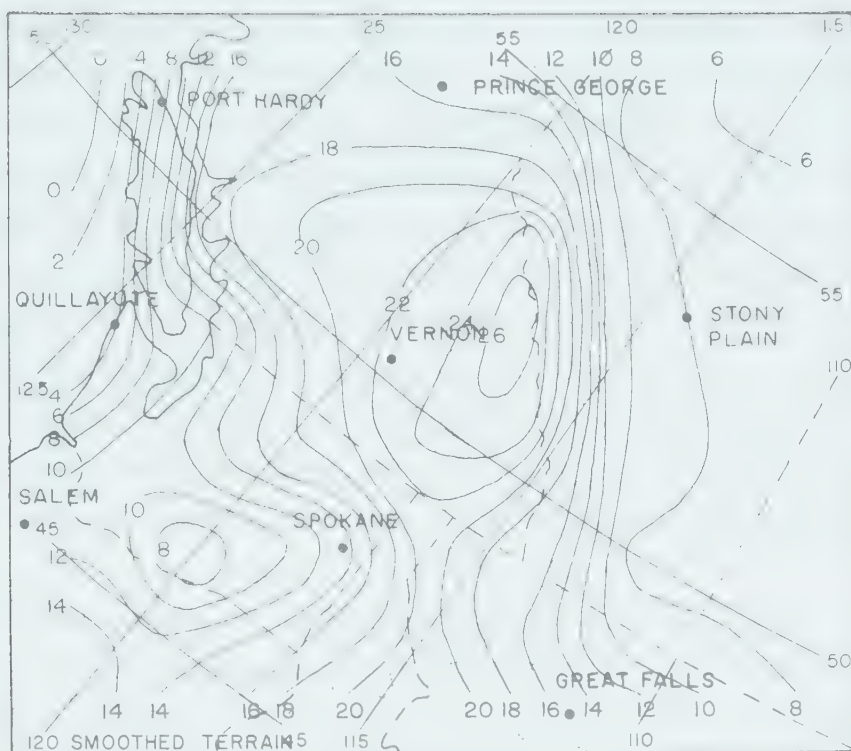


Fig. 7 The smoothed terrain of the area for which the ageostrophic winds were analyzed. Contours are labelled in hundreds of meters above-sea-level.

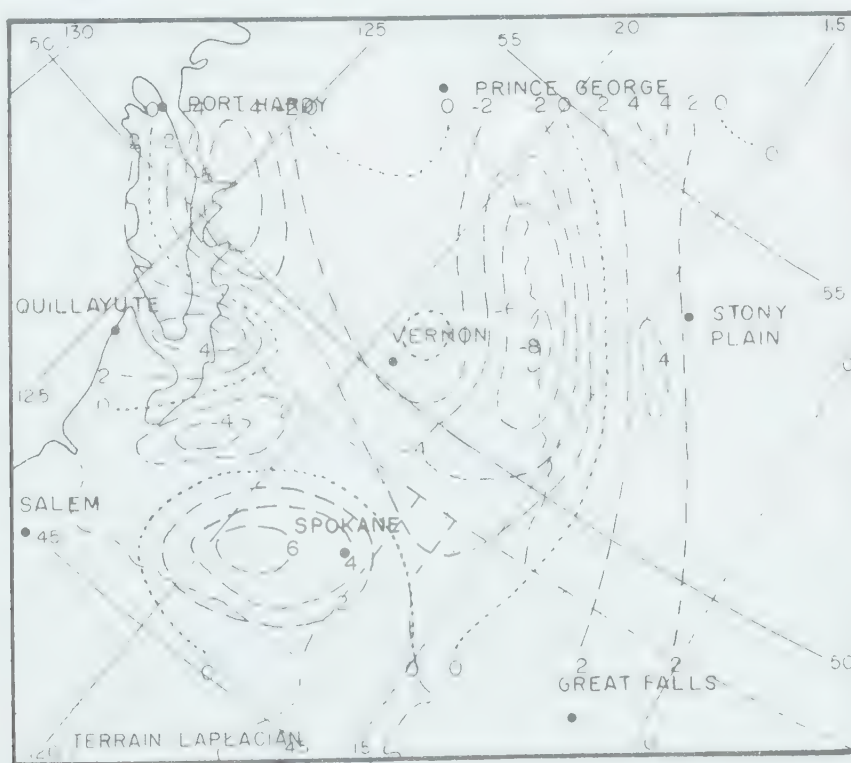


Fig. 8 The Laplacian of the smoothed terrain of Fig. 7 using a finite-difference interval of 185.3 km. Isopleth units are 10^{-8} m^{-1} .

in areas of relatively dense observations the resulting analysis may differ appreciably from geostrophic if the wind and height fields do not agree well with the geostrophic approximation. The balance equation could be a suitable alternative since it involves the use of a stream function, and hence would try to force the resulting analysis to be non-divergent. However, inaccuracies in the observed data, and the necessity of solving a Poisson equation over the grid tend to produce an analysis which does not differ appreciably from that using the geostrophic relationship. To circumvent this problem and effect a considerable saving in computer time only the height field was analyzed and the geostrophic winds were obtained using equations (2.1.3).

The method of analysis consists basically of using the reported data to make successive corrections to an initial guess by making several passes (or scans) over the grid. In this study, the average value of the observed field was used as the first guess to initialize the grid. Bilinear or biquadratic interpolation is used to interpolate from the grid points to the station position. This occasions a change to the individual grid point values from all station observations within a prescribed radius of influence from the grid point. The corrections to the grid values can be made by three different methods:

$$C_1 = \frac{1}{n} \sum_{i=1}^n (O_{x,y} - A_{x,y})_i$$

$$C_2 = \frac{1}{n} \sum_{i=1}^n W_i (O_{x,y} - A_{x,y})_i$$

$$C_3 = \frac{\frac{1}{n} \sum_{i=1}^n W_i (O_{x,y} - A_{x,y})_i}{\frac{1}{n} \sum_{i=1}^n W_i}$$

in which $C_{1,2,3}$ are the corrections to be applied, n is the number of stations affecting the grid point, $O_{x,y}$ is the observed station value, and $A_{x,y}$ is the interpolated station value. The weight function, W_i is the one used by Cressman (1959) and is defined by:

$$W_i = \frac{N^2 - d_i^2}{N^2 + d_i^2}$$

where N is the radius of influence for the scan and d_i is the distance from the i^{th} station to the gridpoint. The radius of influence can be varied for each scan. Corrections of type C_3 lead to a more rapid convergence to the general level of the data within the influence circle.

In regions of sparse data, there is a tendency for discontinuities to develop at the distance where the weight factor approaches zero (i.e. when d_i approaches N). This necessitates the use of a smoothing operator. The one employed is given by:

$$S_{i,j} = \frac{A_{i,j} + b \bar{A}_{i,j}}{1 + b}$$

and

$$\bar{A}_{i,j} = \frac{1}{4} (A_{i+1,j} + A_{i-1,j} + A_{i,j+1} + A_{i,j-1})$$

in which b is a number specified by the programmer and can be varied with each scan, $S_{i,j}$ is the smoothed value of the grid-point values $A_{i,j}$. Clearly, if the smoothing parameter b is zero then no smoothing will be done.

It was necessary to use sixteen passes for the pressure-surface analyses and nine passes for the wind-field analyses in order to produce good agreement with subjectively analyzed samples.

3.5 The Analysis Procedure

The raw data were analyzed as described in Section 3.2, with the pressure height and wind components being extracted at 25 mb intervals from 700 mb to 400 mb inclusive. A time-average of the heights for each level was used as the data input for the objective analysis to obtain the mean flow patterns.

A geostrophic wind at each level for every station and time was obtained by objectively analyzing the height fields and using equations (2.1.3). This allowed u_A and v_A to be computed. A time-average of the ageostrophic components was then calculated for each station and level. The station values of \bar{u}_A and \bar{v}_A were used for the Bellamy calculations. An objective analysis of \bar{u}_A and \bar{v}_A at each level was carried out to calculate the divergence and vorticity by the fundamental method.

CHAPTER IV

THE RESULTS OF THE ANALYSES

4.1 Introduction

In order to reduce boundary effects, and also because centered-space finite differences were employed, the ageostrophic wind components and the relative vorticity and divergence associated with them were computed for a reduced portion of the grid as shown in Figure 9.

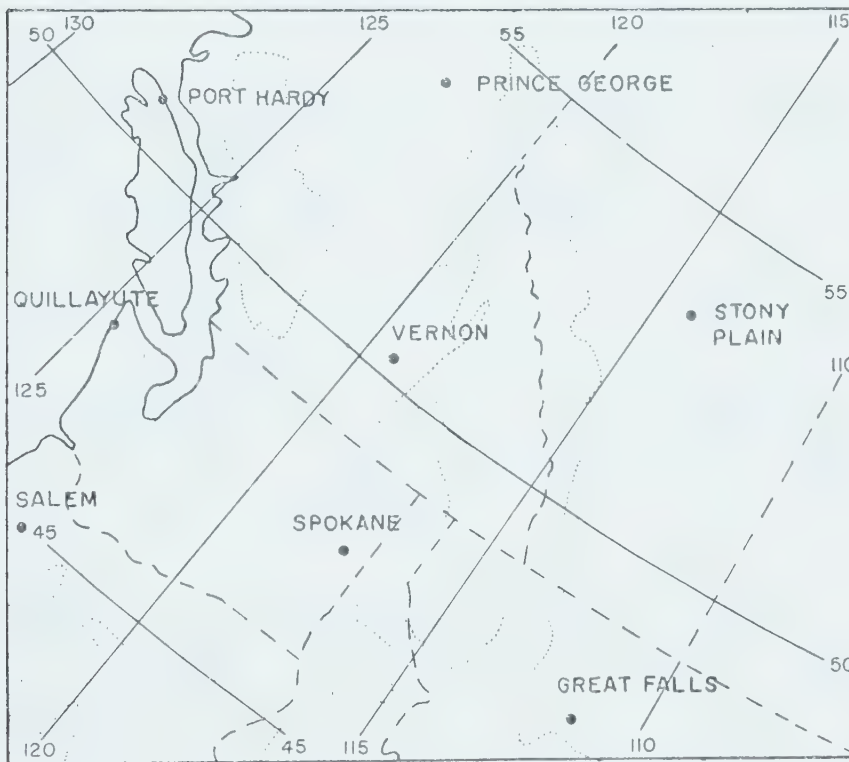


Fig. 9 The geographical area covered by that portion of the grid for which the ageostrophic divergence and relative vorticity were calculated. Thin dotted line is the approximate position of the 1500 m ASL terrain contour.

It should be noted that a reduction was not made over the eastern portions in order to be able to include the lee slopes of the Rocky Mountains.

The results of the divergence and relative vorticity calculations will be presented as vertical averages over the intervals 700-625 mb, 600-525 mb, and 500-400 mb, which will be referred to as the low, middle, and high levels, respectively. Also, for comparison purposes and to make the charts more legible, several transparent overlays are located inside the back cover of the thesis. These include the smoothed contours of the terrain for the reduced grid as shown in Figure 7, the average precipitation areas for the December and January periods studied and shown in Figures 5 and 6, and the terrain Laplacian of Figure 8.

4.2 The Geostrophic Flow for the December Study

The time-averaged geostrophic flow patterns for three levels

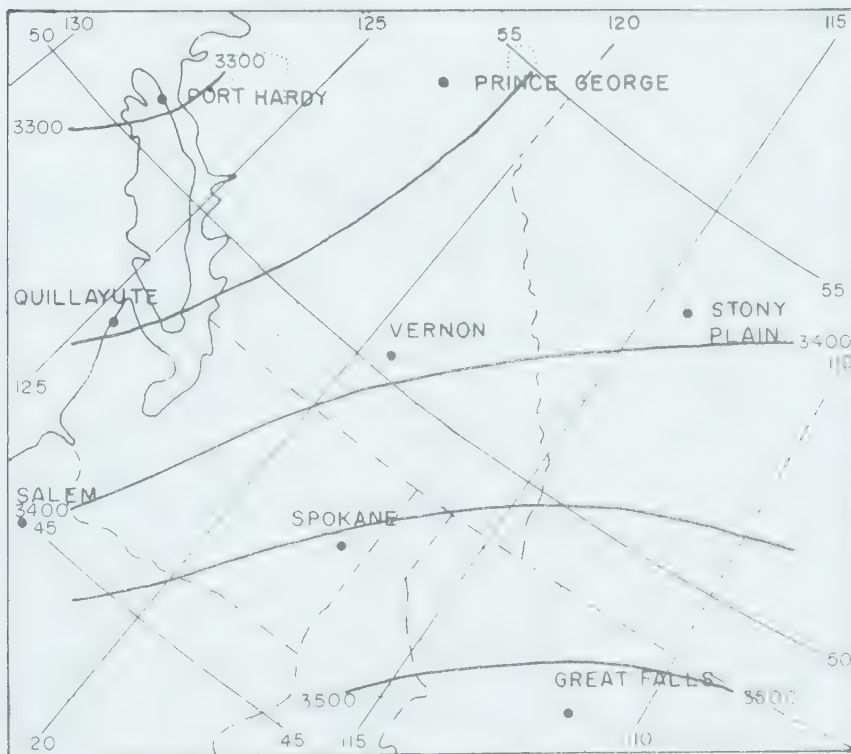


Fig. 10a

Fig. 10 The time-averaged geostrophic flow of the December study for (a) 650 mb, (b) 550 mb, (c) 450 mb. Contour interval is 50 gpm.

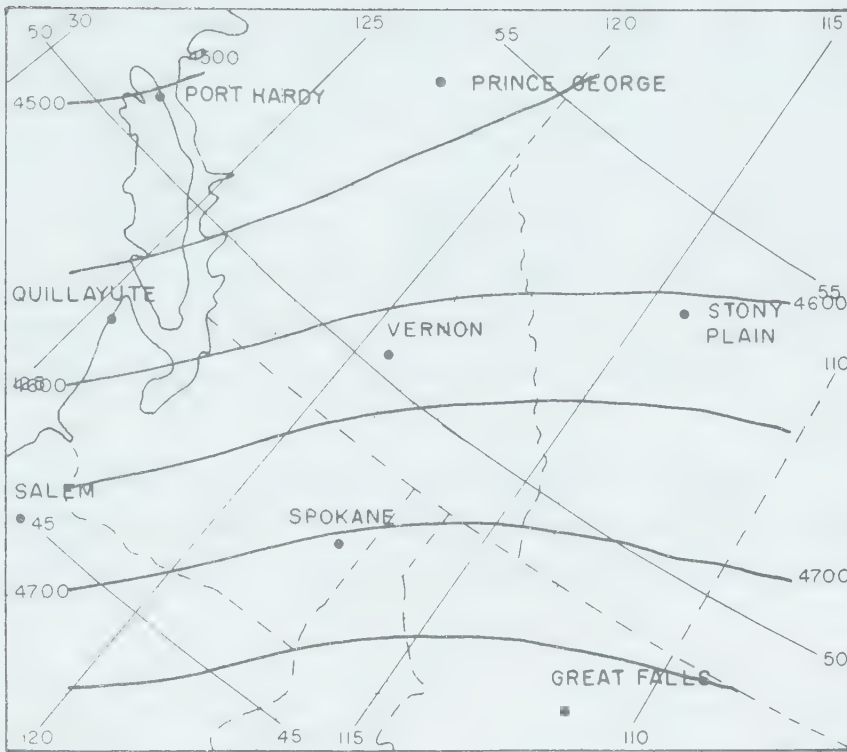


Fig. 10b

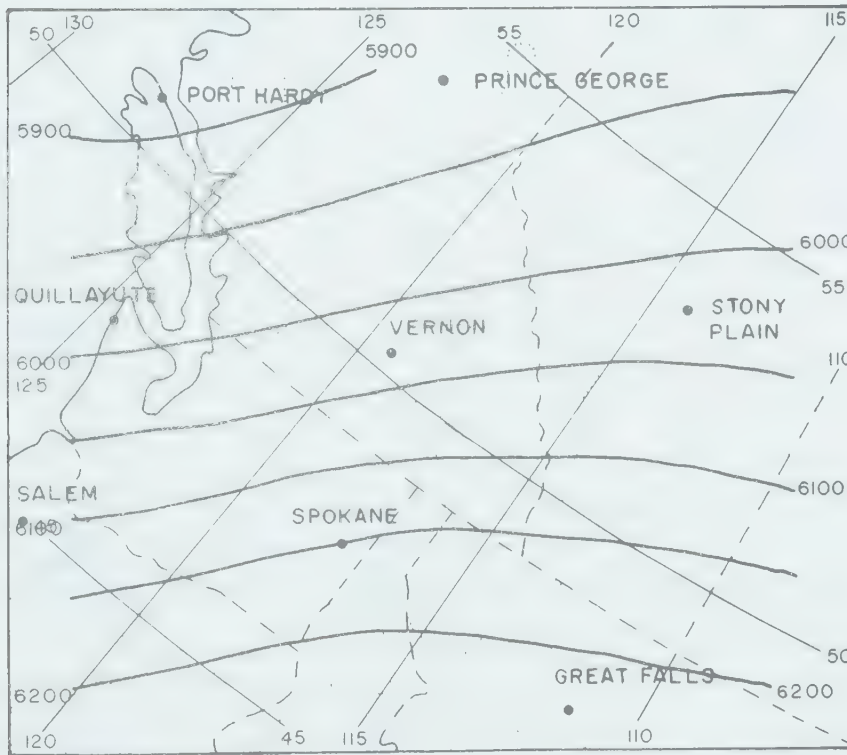


Fig. 10c

The flow shows reasonably constant directions at all levels. Maximum geostrophic winds at all levels were found over the Washington area with values ranging from 20 m sec^{-1} at 700 mb to 30 m sec^{-1} at 400 mb. The average position of the upper low is indicated to be northwest of Vancouver Island. Confluent flow occurs along the coast to the east of Vancouver Island while diffluence is prevalent over the area east of 120°W . Weak ridging occurs at all levels in the vicinity of the Alberta portion of the Rocky Mountains.

4.3 The Ageostrophic Wind Fields of the December Study

The direction of the time-averaged ageostrophic deviations showed little change with height as shown by the samples in Figure 11.

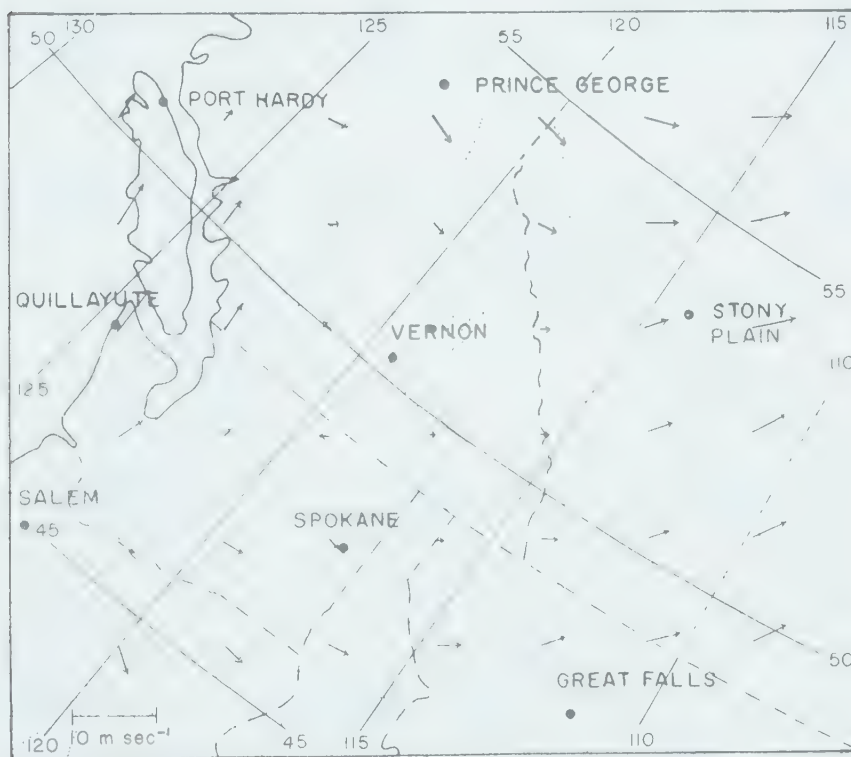


Fig. 11a

Fig. 11 The time-averaged ageostrophic wind components of the December study for (a) 650 mb, (b) 550 mb, (c) 450 mb.

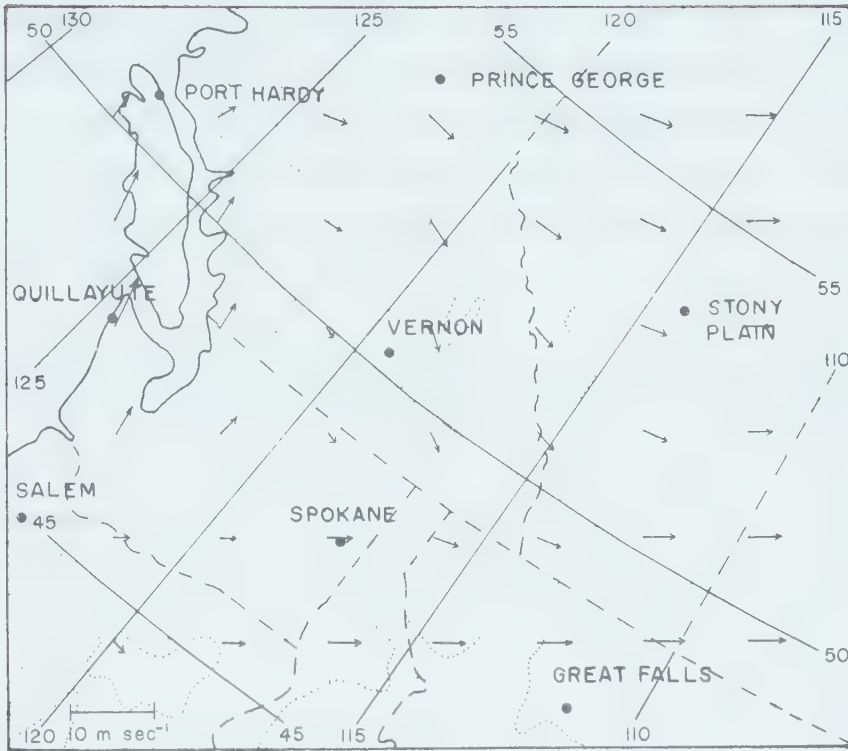


Fig. 11b

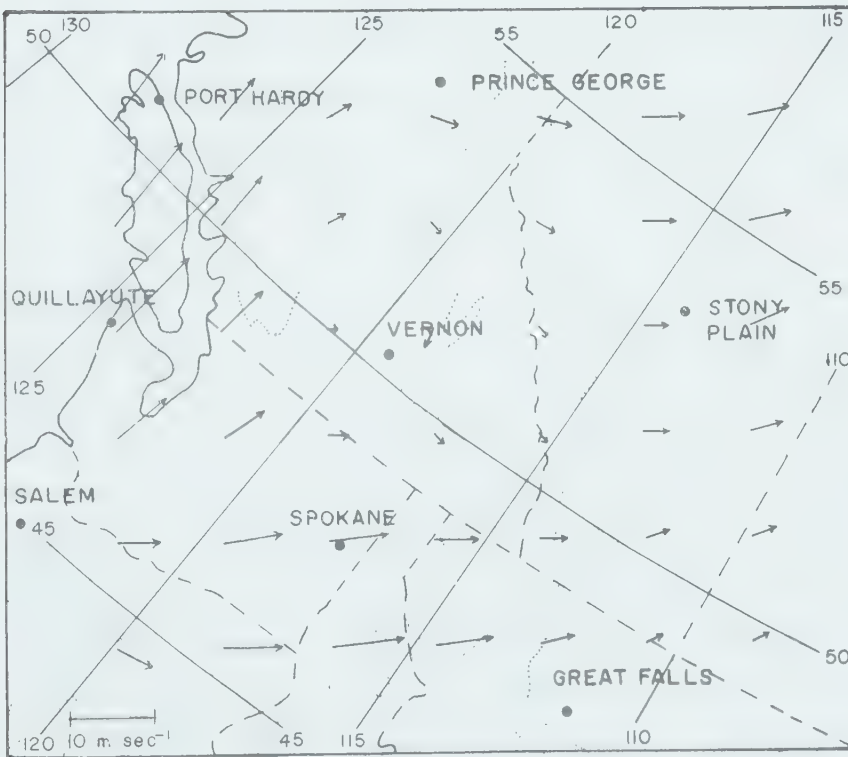


Fig. 11c

The strongest ageostrophic winds were found over Vancouver Island, reaching maximum speeds of 14 m sec^{-1} at 400 mb. Comparison with Figure 10 shows that the ageostrophic component over Vancouver Island is predominantly across the contours toward lower contour values. Although the geostrophic winds show a general increase in speed at progressively higher levels, a similar trend is not apparent in the ageostrophic winds.

4.4 The Ageostrophic Divergence Fields of the December Study

The difference found by subtracting the divergence calculated by the fundamental method from that obtained by Bellamy's technique was obtained at the positions of the Bellamy triangle centroids for each level. The resulting 78 values had a mean of $0.4 \times 10^{-6} \text{ sec}^{-1}$ with a standard deviation of $11.2 \times 10^{-6} \text{ sec}^{-1}$. A comment on these results is necessary. To compare the results in this manner is not strictly valid since the fundamental method and Bellamy method use different regions of data to compute the vorticity and divergence. In spite of this, a difference in sign occurred at only 14 of the 78 available points. If the Bellamy values were incorporated with the fundamental values by some method, the results would show only minor changes from those obtained by the fundamental method alone. Hence, only the fundamental results are presented in Figure 12 because of the more complete coverage obtained over the area of concern.

The major convergence cell near 50°N , 125°W fits well with the previously noted confluent mean flow over this area. Similarly, the divergence area over Alberta is reflected by the diffluent nature of the mean flow over the eastern portions of the grid. The divergence cell centered near 46°N , 122°W is surprisingly strong considering the weak diffluence of the mean flow in this area. Gradient wind contributions can only account for about 20-25% of the observed values. Estimated gradient wind contributions over Montana and the extreme southern portions of Alberta ranged from $-2 \times 10^{-6} \text{ sec}^{-1}$ in the low levels to $-4 \times 10^{-6} \text{ sec}^{-1}$ in the higher levels. The gradient wind

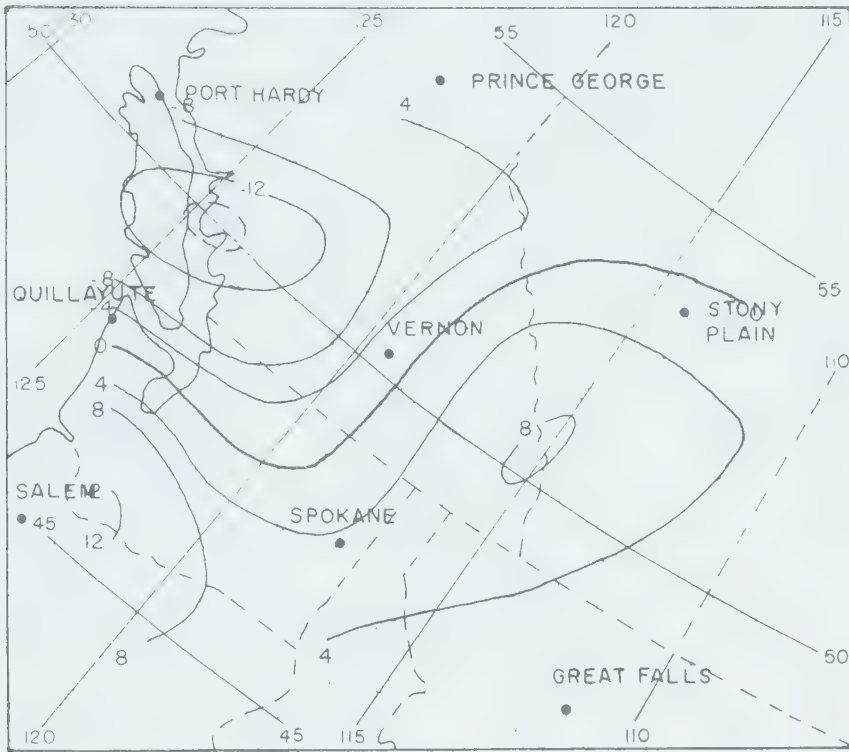


Fig. 12a

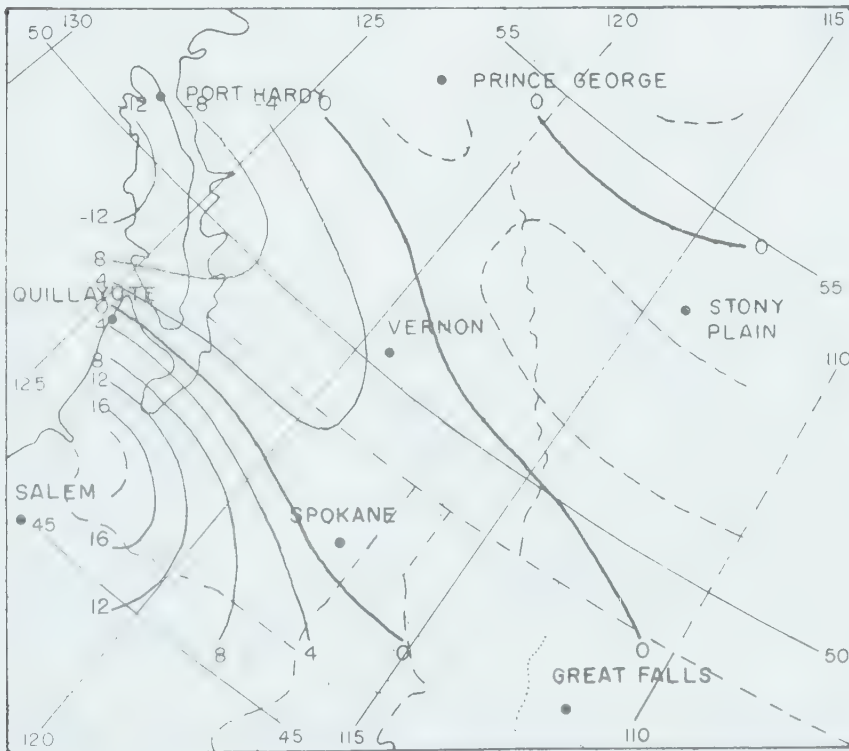


Fig. 12b

Fig. 12 The ageostrophic divergence fields of the December study as calculated by the fundamental method for (a) low levels, (b) middle levels, (c) high levels. Isopleths are in units of 10^{-6} sec^{-1} .

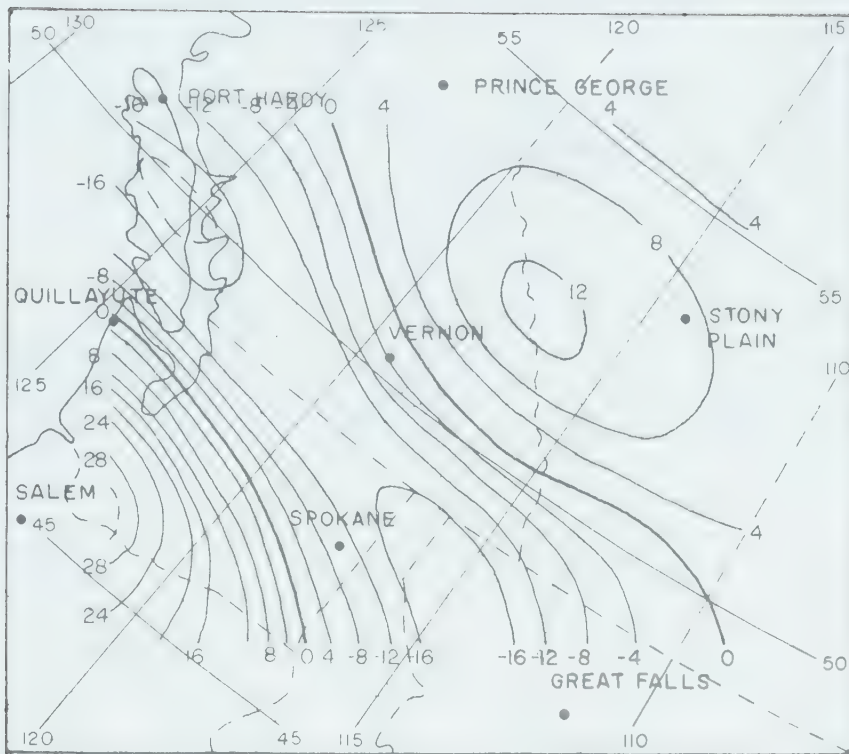


Fig. 12c

cannot account for the strong nature of the secondary convergence cell which appears in the high levels over Idaho, although it is probably a contributing factor. The northward shift with height of the secondary divergence cell which is centered over 51°N , 115°W at low levels is accompanied by a weakening in the middle levels as it passes through the region of gradient wind induced convergence. A marked increase in the intensity of this cell is shown in the high levels as it moves out of the area of gradient wind influence.

4.5 The Ageostrophic Relative Vorticity Fields for the December Study

A comparison of the Bellamy and fundamental results by the method described in Section 4.4 gave a mean difference of $-0.2 \times 10^{-5} \text{ sec}^{-1}$ with a standard deviation of $0.7 \times 10^{-5} \text{ sec}^{-1}$. As with

the divergence values, the difference of the vorticity values was primarily one of magnitude -- not of sign. Hence only the fundamental results are presented in Figure 13.

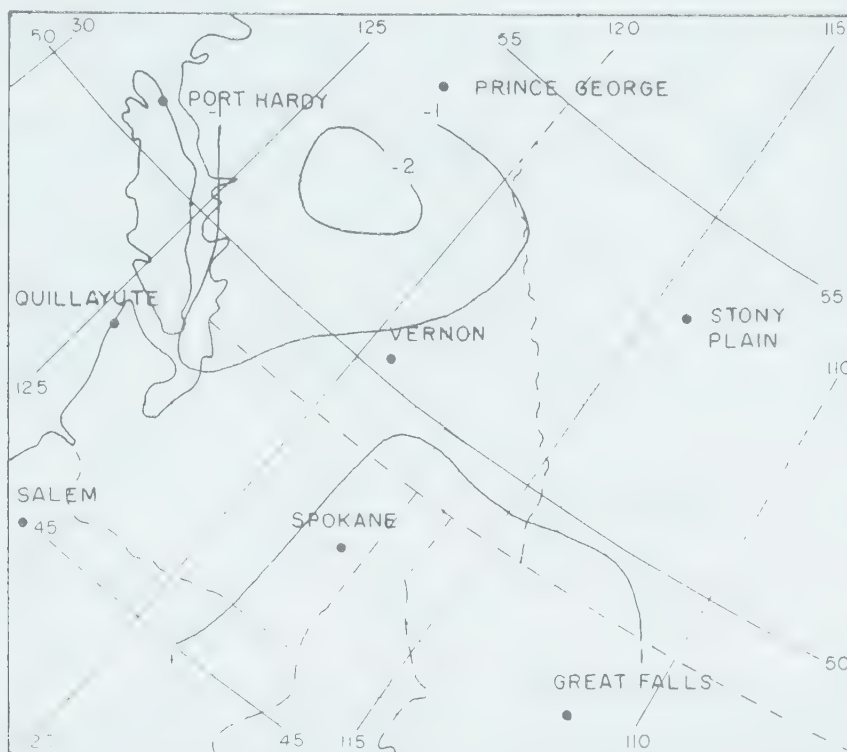


Fig. 13a

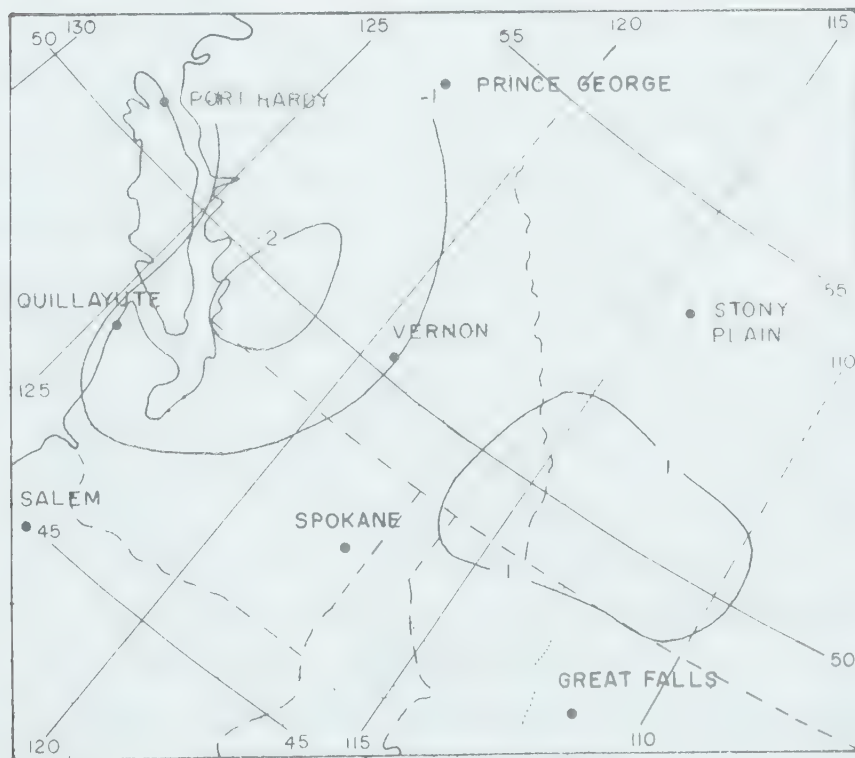


Fig. 13b

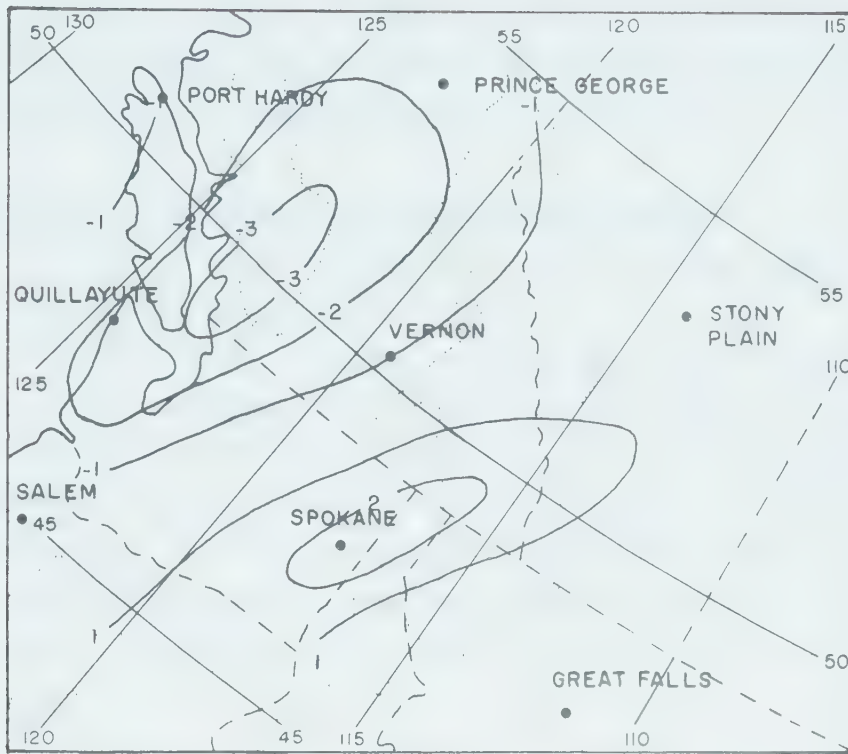


Fig. 13c

Fig. 13 The ageostrophic relative vorticity fields of the December study as calculated by the fundamental method for (a) low levels, (b) middle levels, (c) high levels. Isopleths are in units of 10^{-5} sec^{-1} .

When compared with the mean geostrophic flow of Figure 10, one finds that the ageostrophic relative vorticities have the opposite "polarity" to that expected from the geostrophic motions. It should be noted that this difference would probably not be reflected in the geostrophic vorticity field since it is of order 10^{-4} sec^{-1} , while the ageostrophic vorticities are of order 10^{-5} sec^{-1} .

A comparison of the low-level vorticity pattern with the terrain Laplacian of Figure 8 shows good agreement for the region of negative vorticity, but poor agreement for the area of positive vorticity. The middle and upper levels show little correlation with the terrain Laplacian. It is possible that the vorticity patterns, and by direct association also the ageostrophic deviations, arise in part from the mean geostrophic flow trying to conserve its absolute vorticity, since air moving northward would tend to gain negative relative vorticity. This would account for the stronger negative

vorticity values since the components of northward deviation are considerably stronger than the southward components.

4.6 The Mean Geostrophic Flow for the January Study

As indicated by Figure 14, there is little change in the mean flow patterns with height.

At low levels there is confluent flow over Vancouver Island extending east to roughly 120°W , and generally diffluent flow over Alberta. The middle and high levels show a strengthening of the flow. The confluent zone of the low-level flow disappears at higher levels, but there is still some indication of diffluence over Montana and the eastern portions of Alberta. Maximum geostrophic wind speeds ranged from 25 m sec^{-1} at 700 mb to 45 m sec^{-1} at 400 mb.

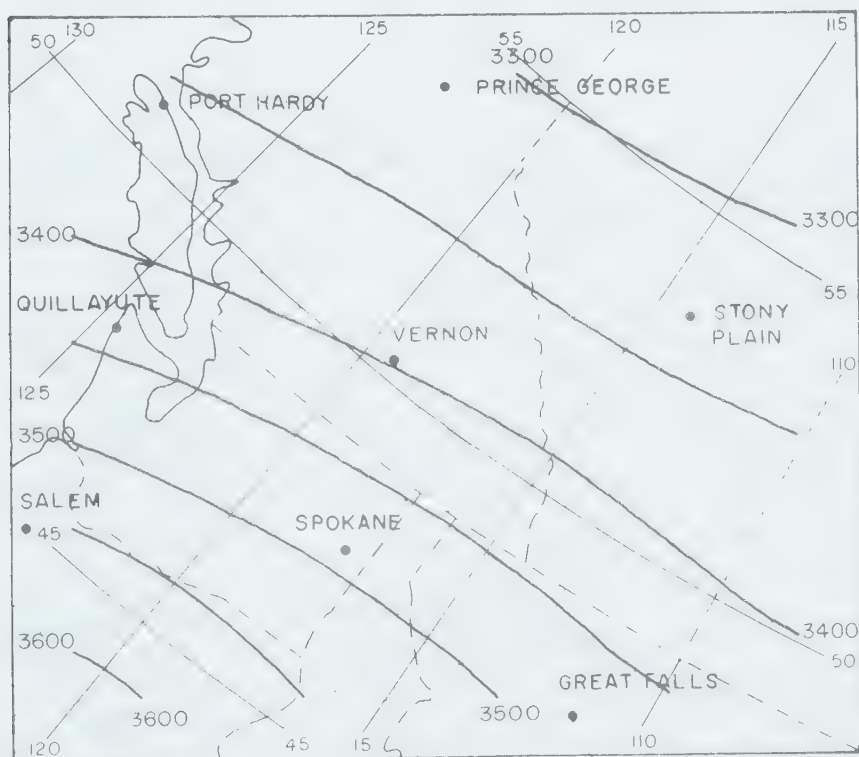


Fig. 14a

Fig. 14 The time-averaged geostrophic flow of the January study for (a) 650 mb, (b) 550 mb, (c) 450 mb. Contour interval is 50 gpm.

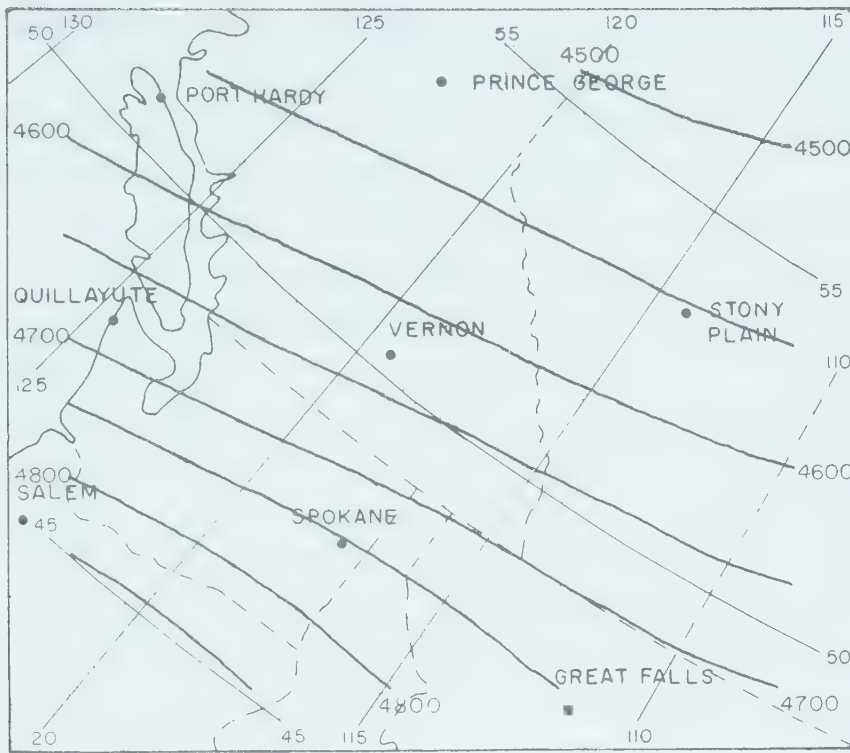


Fig. 14b

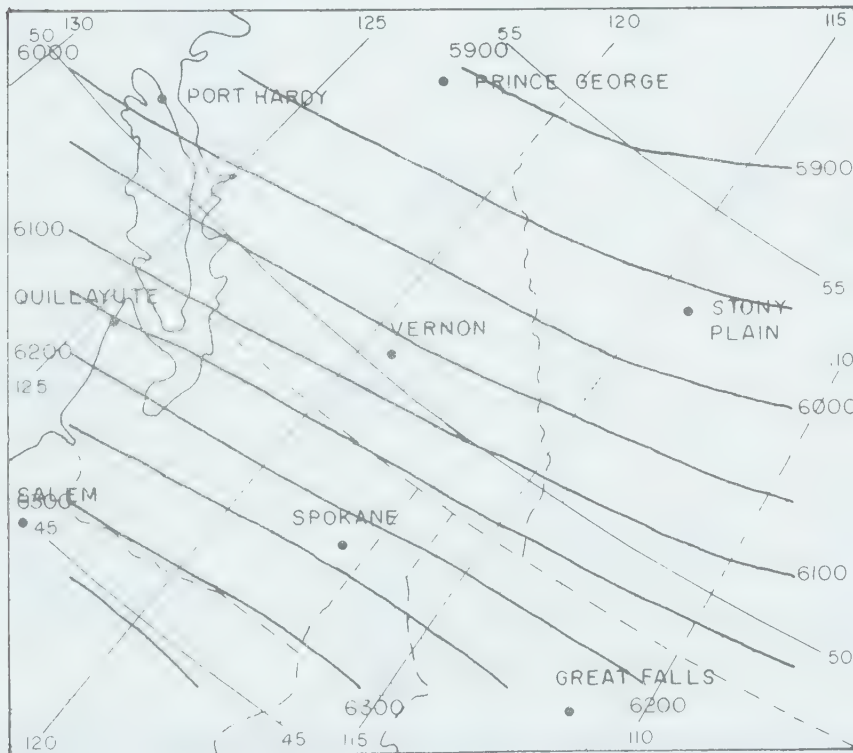


Fig. 14c

4.7 The Mean Ageostrophic Deviations for the January Study

The mean ageostrophic deviations for the January case study for which samples are shown in Figure 15 do not exhibit the same degree of consistency with height found in the December case.

The most notable change occurs in the vicinity of Vancouver Island. A basically geostrophic low-level flow is indicated by the relatively small westward ageostrophic winds in this area. A southward component appears over this area in the middle levels which increases in strength with height up to the 400 mb level. Other areas of the grid show the same basic features at all levels -- southward deviations over the eastern portions of Alberta, and east to northeastward deviations over Idaho and Montana. The center of small deviations near Edmonton in the low and middle levels shifts to the southwest at high levels to a position near Vernon, B.C. Small ageostrophic components are found at all levels over the southern portions of Washington State.

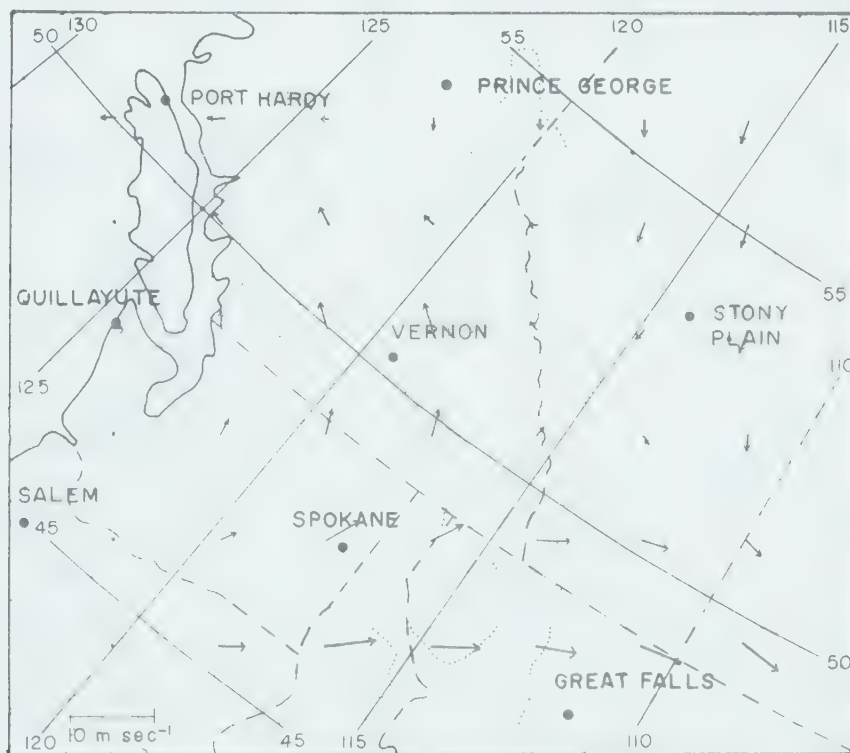


Fig. 15a

Fig. 15 The time-averaged ageostrophic wind components of the January study for (a) 650 mb, (b) 550 mb, (c) 450 mb.

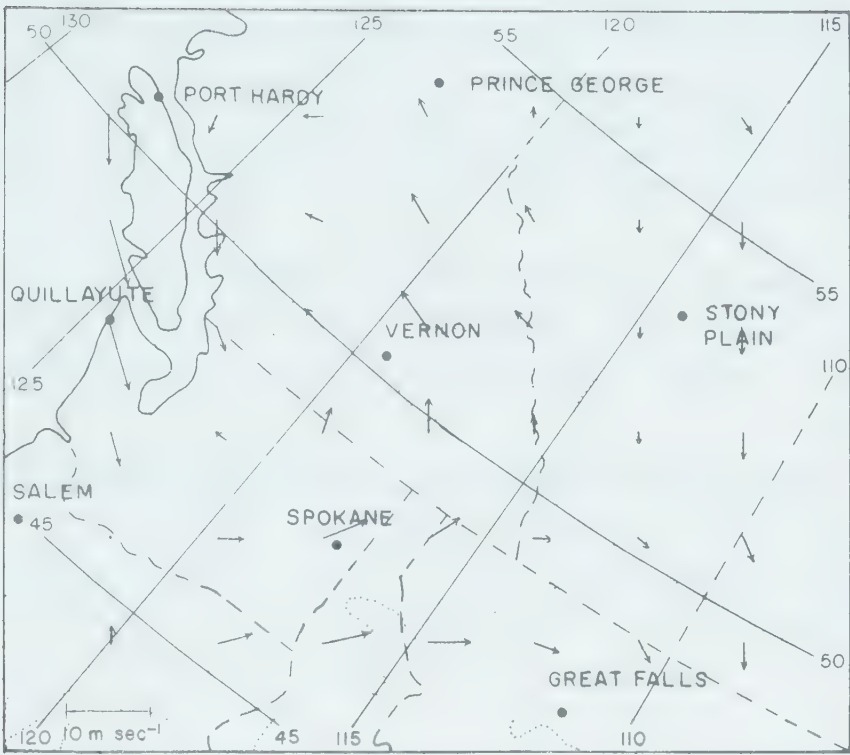


Fig. 15b

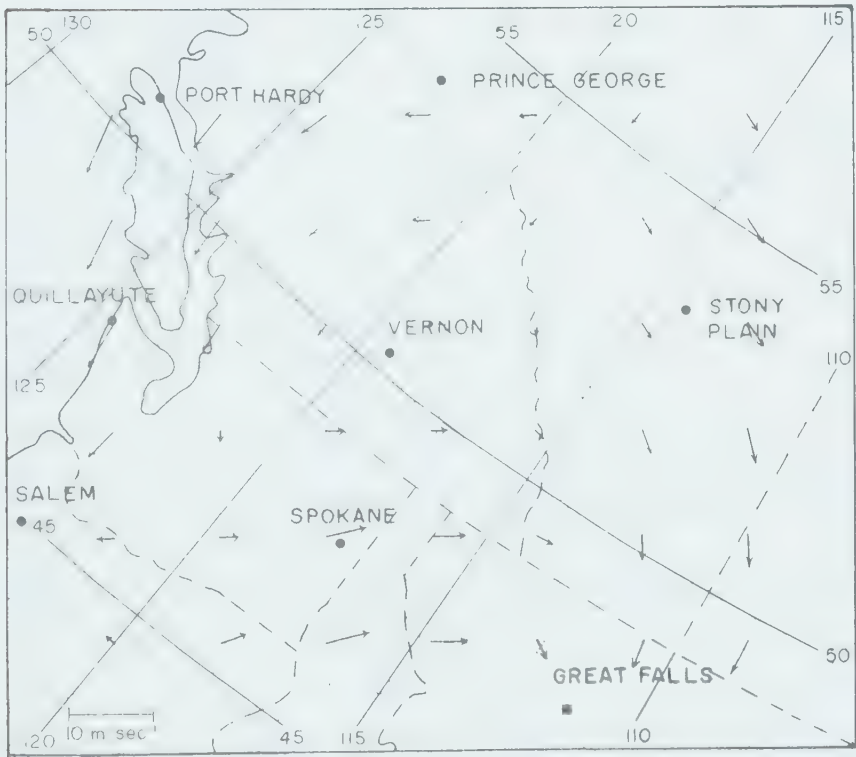


Fig. 15c

The ageostrophic winds above Idaho, Montana, and the eastern portions of Alberta indicate a strong to moderate cross-contour flow at all levels. The strong southward ageostrophic component above 600 mb around Vancouver Island also gives strong cross-contour flow in this area.

The cross-contour flow over Alberta and Vancouver Island is interesting in that it is directed towards higher geopotential, making it difficult to interpret as a frictional effect.

4.8 The Ageostrophic Divergence Fields of the January Study

The fundamental results are presented in Figure 16. The ageostrophic divergence values of the Bellamy method show good agreement with these results, having a mean difference of $1 \times 10^{-6} \text{ sec}^{-1}$ with a standard deviation of $6 \times 10^{-6} \text{ sec}^{-1}$.

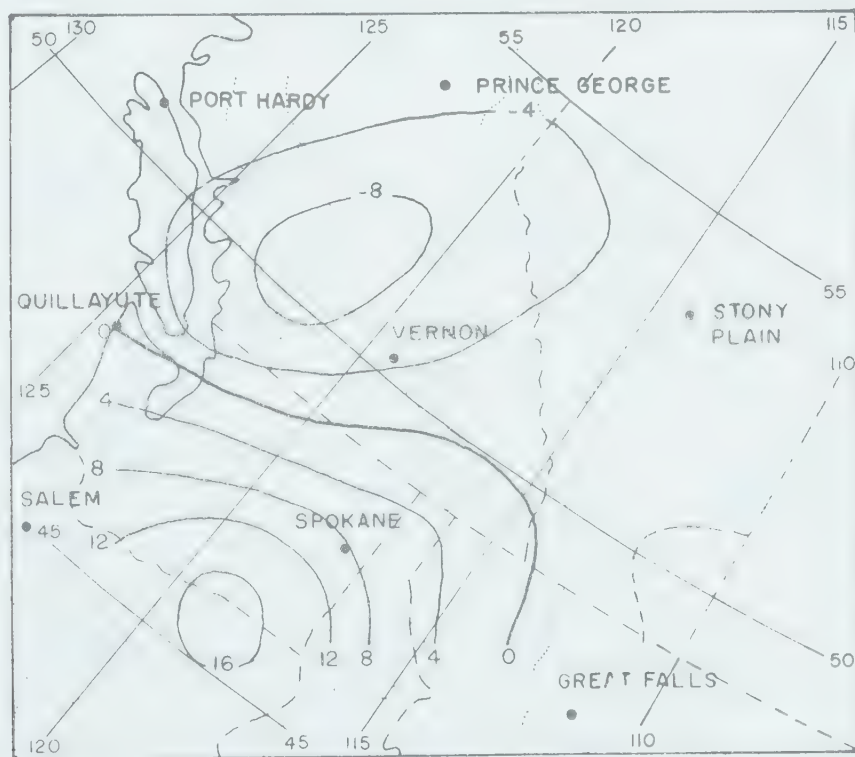


Fig. 16a

Fig. 16 The ageostrophic divergence fields of the January study as calculated by the fundamental method for (a) low levels, (b) middle levels, (c) high levels. Isopleths are in units of 10^{-6} sec^{-1} .

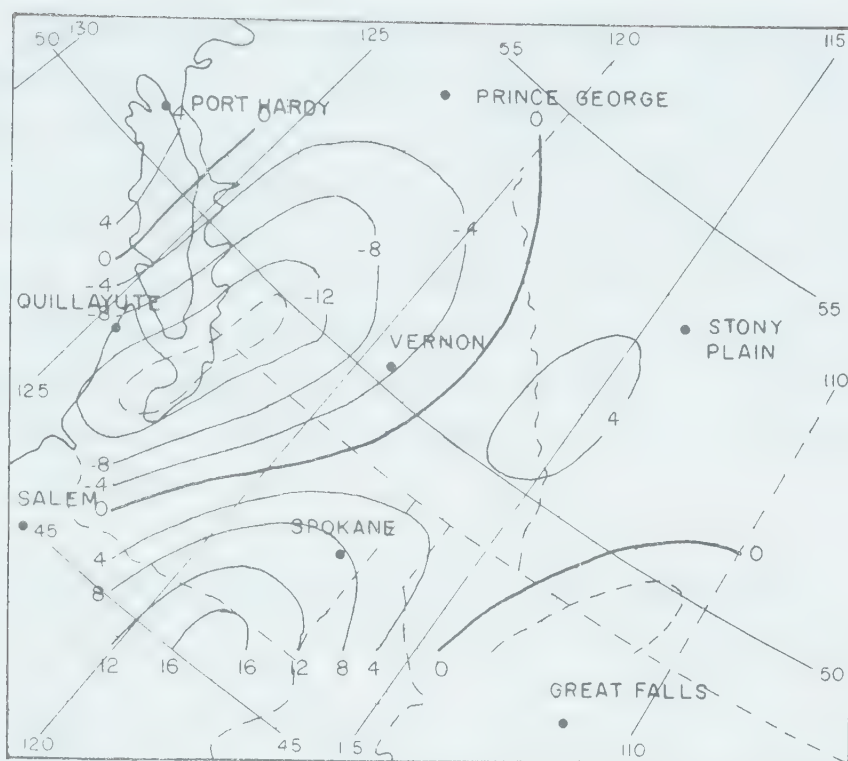


Fig. 16b

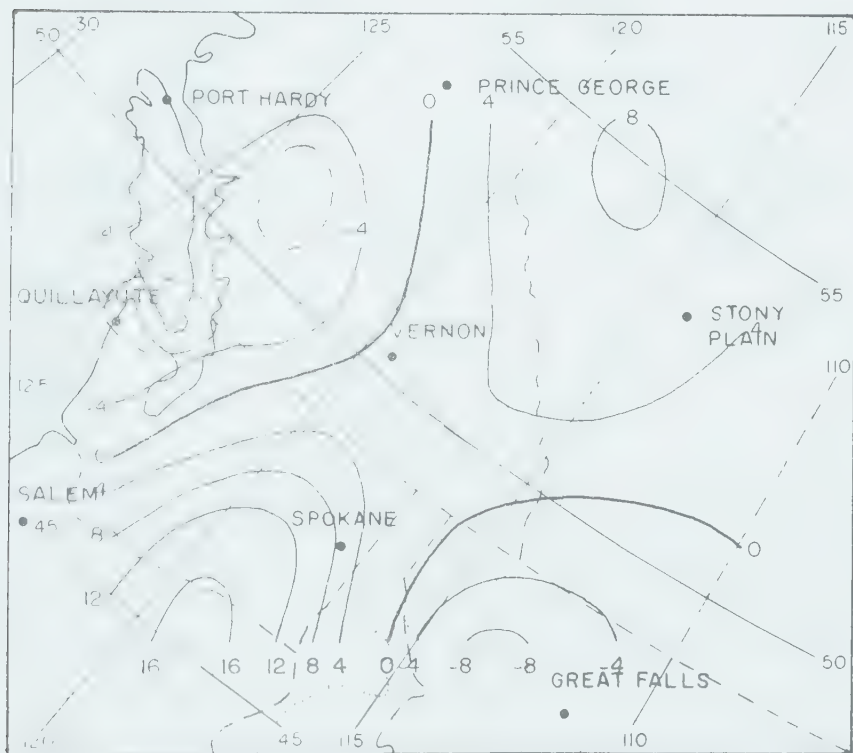


Fig. 16c

The low-level results show a center of convergence near 50°N , 122°W and a center of divergence near 46°N , 118°W , with convergence prevailing over Alberta and British Columbia. The appearance of the southward ageostrophic component over Vancouver Island above 600 mb results in a southwest shift of the main convergence center which reaches maximum intensity through the middle levels. The middle and high levels also show the appearance of secondary centers of convergence and divergence over Montana and Alberta, respectively. The weak curvature of the mean flow resulted in negligible gradient-wind effects at all levels.

4.9 The Ageostrophic Vorticity Fields of the January Study

The difference found by subtracting the fundamental results from the Bellamy results had a mean value of $-0.2 \times 10^{-5} \text{ sec}^{-1}$ with a standard deviation of 1×10^{-5} . The two sets of results showed good agreement in sign. The fundamental results are given in Figure 17.

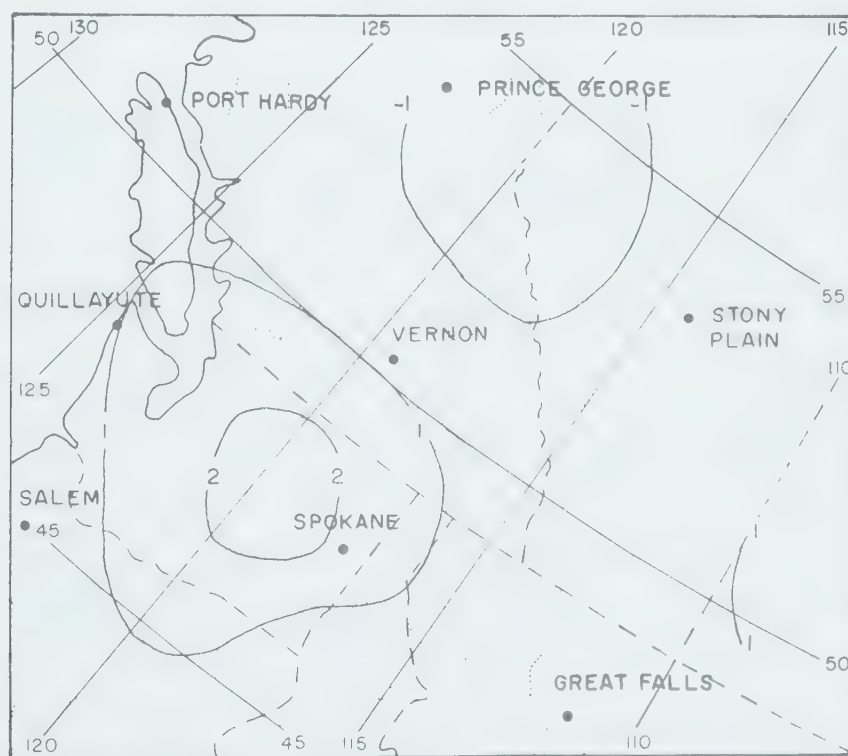


Fig. 17a

Fig. 17 The ageostrophic relative vorticity fields for the January study as calculated by the fundamental method for (a) low levels, (b) middle levels, (c) high levels. Isopleths are in units of 10^{-5} sec^{-1} .

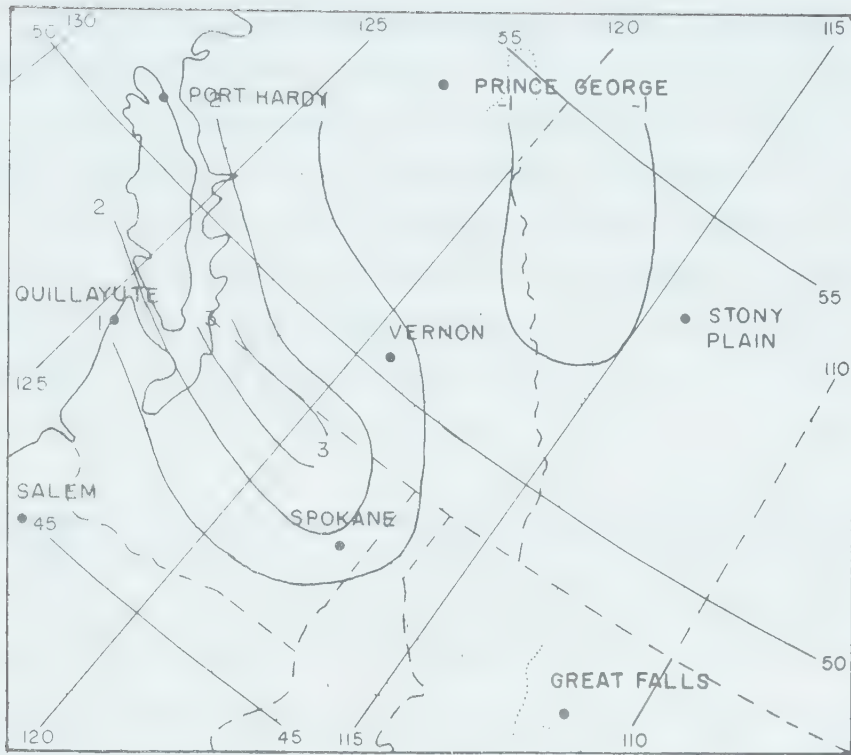


Fig. 17b

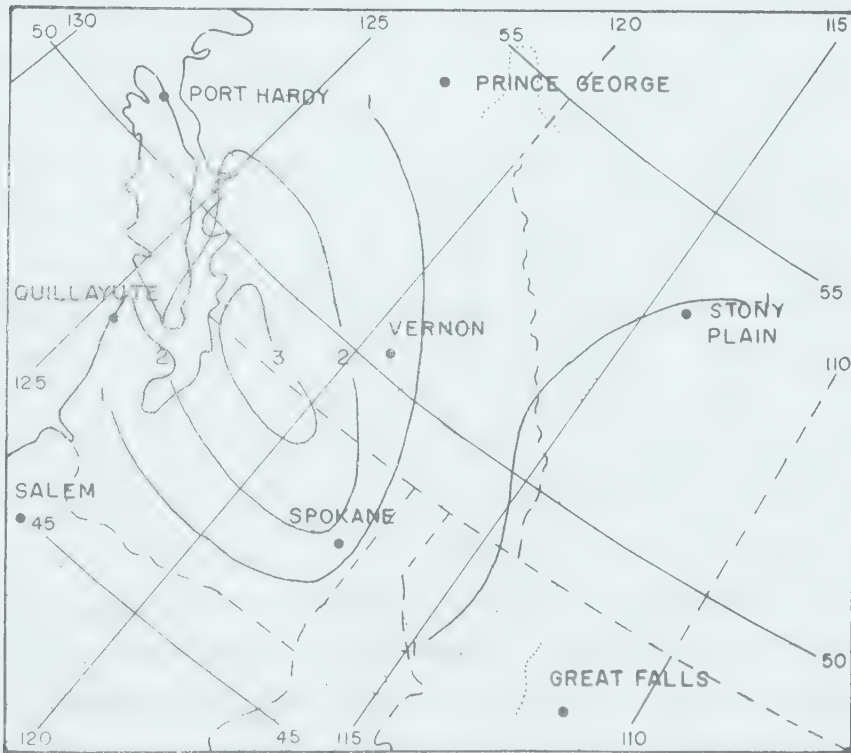


Fig. 17c

The strong southward ageostrophic wind components in the middle and high levels over Vancouver Island are reflected in the northwest shift, and increase in strength at these levels of the positive center which appears in the low levels over the Central Washington area.

While the low-level vorticity pattern shows some correlation with the terrain Laplacian of Figure 8, the agreement is poor in the upper levels. As with the December case, the relative vorticity of the ageostrophic deviations is of the opposite sign to that of the mean flow in the same areas.

4.10 Terrain and Condensational Heating Influences in the Results

The main objective in undertaking this investigation was to try and detect terrain influence in the wind field at levels where direct interference by the terrain would not occur. Unfortunately, attempts to correlate the calculated ageostrophic deviations with the terrain features of Figure 7 were unsuccessful, with two possible exceptions. These exceptions involve the small area of precipitation located near 49°N , 122°W which occurred in both the periods investigated. An examination of the soundings for Port Hardy and Quillayute during the January period indicated latent instability in the levels near the surface which could be triggered by the forced ascent encountered by the air in these low levels as it surmounted the Coast Range. Air rising due to this instability could not penetrate much above 600 mb because of a strong inversion from this level to about 500 mb. The latent heat released by condensation in this rising air and the resulting precipitation may account for part of the low-level convergence over this area. However, Aubert (1957) has shown that the largest values of convergence generated by condensational heating should occur below the level of greatest condensation. Hence, the observed maximum of convergence over this area in the 600 to 525 mb levels cannot be explained by either terrain or condensational heating effects. An analysis of the secondary center of precipitation for the December study produced similar results, with the exception that the factor inhibiting vertical motions was a lapse rate somewhat less than pseudo-adiabatic above 550 mb.

The soundings for the other stations in that portion of the grid for which ageostrophic winds were calculated showed that Port Hardy and Quillayute were the only stations for both periods with any significant degree of instability present. This implies that terrain effects were probably of a very minor nature at the levels analysed.

The major precipitation area which occurred over Alberta during both the December and January periods was caused by weak frontal activity in the 850 to 700 mb layers and may account for the weak convergence in the lower layers over Alberta during the January period.

It is apparent that some other controlling influence must be present that was not considered in Chapter II. The effects of horizontal thermal advection have been neglected to this point and will now be examined with regard to the results.

4.11 Thermal Advection Effects for the December Study

The December soundings for the stations enclosed by or bordering on the reduced grid of Figure 9 were examined for evidence of horizontal thermal advection. When the results of this investigation were compared with the computed ageostrophic deviations of Figure 11, it was found that in general, a southward ageostrophic component occurred with cold advection, while a northward component occurred with warm advection. In the light of these occurrences, the effects of a strong but slowly moving trough of warm air aloft which moved inland from the Pacific during the period are shown by the warm advection above and to the west of Vancouver Island. This warm advection is responsible for the strong ageostrophic convergence around Vancouver Island. The relatively light ageostrophic winds over Washington are a result of the time-averaging procedure. However, the strong divergence over this area reflects the dominant effect of cold advection following the passage of the trough of warm air. Warm advection in the middle and high levels accounts for the secondary cell of convergence found at these levels. The weak warm advection above 700 mb over Alberta and the Prince George area is off-set by strong advection of cold air below this level resulting in net ageostrophic divergence.

4.12 Thermal Advection Effects for the January Study

As one might expect from the rather complicated pattern of the ageostrophic winds for the January study, thermal advection was somewhat more difficult to determine from the soundings. However, several features were apparent. The southward deviations over Alberta accompanied cold advection at all levels and resulted in the divergence which appears in the middle and high layers. As noted in Section 4.10, the low level convergence may be due to condensational heating effects.

The soundings for Prince George and Port Hardy indicated that the strong southward ageostrophic component which develops over and to the west of Vancouver Island above 600 mb accompanies the advection of a warm dry air mass into this area at these levels, while weak cold advection was present below 650 mb. The narrow swath of ageostrophic winds having a northward component found over central British Columbia at all levels up to 500 mb was caused by strong warm advection below 500 mb in this area during the first half of the period. Thus, the convergence area which appears over most of British Columbia, Vancouver Island, and the northwest portions of Washington is a simple consequence of a rather complex thermal advection pattern.

4.13 Summary of the Results

The time-averaged ageostrophic wind components that were calculated show reasonable agreement with the characteristics outlined in a general study by Godson (1950). The divergence values calculated from the ageostrophic winds lie in the generally accepted range of 10^{-6} sec^{-1} to 10^{-5} sec^{-1} for synoptic scale atmospheric motions. The ageostrophic relative vorticities, with magnitudes of order 10^{-5} sec^{-1} conform to the normal assumption that the divergent component of the wind field has a relative vorticity which is one order of magnitude less than that of the rotational (i.e. quasi-geostrophic) component which is of order 10^{-4} sec^{-1} .

There appears to be a weak contribution by condensational heating to the low level convergence found over Alberta during the period of the January study. Condensational heating may also contribute to the low level convergence found over British Columbia in both periods

studied. Gradient winds had a small effect on divergence areas over Washington and Alberta during the December periods, but were negligible during the January period.

It is felt that the apparent absence of terrain influence throughout the 700-400 mb layer during both periods may be caused by the stability of the atmosphere over the area studied. The correlation between thermal advection and the regions of ageostrophic divergence and convergence suggests that horizontal thermal advection was the influence controlling the ageostrophic deviations.

CHAPTER V

SUMMARY AND CONCLUSIONS, WITH SOME SUGGESTIONS FOR FURTHER WORK

5.1 Summary of the Methods Employed and the Calculated Results

Two methods were outlined that are suitable for calculating the divergence and relative vorticity of the ageostrophic wind. The first method is referred to as the fundamental method and is based on the kinematic definitions of divergence and vorticity. The second technique is one developed by Bellamy (1949), and was intended primarily as a check on the values found using the fundamental methods. The merits and drawbacks of the two methods were discussed and it was decided to use the time-averaged ageostrophic wind fields for both methods in order to reduce the effects of observational errors.

The ageostrophic component of the observed wind was obtained by subtracting an objectively analyzed geostrophic component from the observed wind. Possible sources of the ageostrophic wind component were discussed, including atmospheric compressibility, the gradient wind, diabatic heating by condensation, and terrain influences. Quantitative estimates of the contributions these factors could make to the ageostrophic divergence and relative vorticity were obtained where possible. A rough estimate was obtained of the uncertainty in the vorticity and divergence caused by errors in the observations, indicating that the values obtained by the Bellamy technique will generally be less uncertain than those of the fundamental method.

Two case studies of the ageostrophic wind field were presented: one from December 1971, and the other from January 1972. For objective analysis purposes, and to facilitate the computations, a finite-differencing grid covering the geographical area studied was employed. The portion of the grid for which the ageostrophic divergence and relative vorticity were calculated included the southern portions of British Columbia and Alberta, the state of Washington, and portions

of Idaho and Montana. A smoothed topography for the terrain of these areas was obtained, and the Laplacian of this topographical surface was computed.

Using the original radiosonde ascent recordings, the geopotential heights of the pressure surfaces from 700 to 400 mb at 25-mb intervals, as well as the corresponding wind vectors, were obtained at each observing station within the area covered by the grid, giving a total of thirteen levels. A time-average of the calculated heights for each level at each station was used to obtain the objectively analyzed mean flow for each of the two periods. The geostrophic wind was obtained for each station at every level and time using objective analysis and finite-difference techniques. This permitted the computation of the ageostrophic winds at the desired levels for each station and time. A time-average was taken of the ageostrophic components and used to calculate the Bellamy values of the ageostrophic divergence and vorticity. An objective analysis of these average ageostrophic components permitted the calculation of the fundamental values for the vorticity and divergence.

The time-averaged ageostrophic wind fields for both periods conformed to the normal assumption that the divergent portion of the observed wind is generally an order of magnitude less than the rotational portion. Cross-contour components appeared at all levels over various portions of the grid. The sign of the Bellamy and fundamental results showed generally good agreement, with acceptable differences in magnitude. The ageostrophic divergence values occurred in the synoptically acceptable range of $\pm 10^{-6}$ to $\pm 10^{-5} \text{ sec}^{-1}$, while the ageostrophic relative vorticities were of the order of $\pm 10^{-5} \text{ sec}^{-1}$.

Condensational heating appeared to contribute to convergence in the 700 to 625-mb layer over Alberta during the January period. Diabatic heating may also have given some low level support to the convergence which occurred over British Columbia during both periods. Ageostrophic components arising from the gradient wind had a minor effect on the divergence fields during the December period, but were negligible for the January case.

No correlation was evident between the ageostrophic wind fields and the terrain, while the ageostrophic vorticities showed fair agreement with the terrain Laplacian in only the lowest levels studied. The ageostrophic winds and the divergence fields derived from them did show a good correlation with horizontal thermal advection that occurred during the periods studied, suggesting that this was the influence controlling the ageostrophic deviations for both periods.

5.2 Conclusions

No conclusions could be drawn on the nature of terrain influences in the upper flow during the periods studied. However, this does not mean that terrain effects were not present -- rather that the methods employed, the data available, and the prevailing atmospheric stabilities did not permit sufficient resolution of the wind field to be able to detect the results of terrain influence. The low level nature of the precipitation which occurred, and the calculated mean flow patterns resulted in only minor effects from the influences of condensational heating and the gradient wind.

The rather unexpected ability of horizontal thermal advection to account for the dominant features of the ageostrophic divergence fields of both periods strongly suggests that this was the controlling influence on the ageostrophic wind fields. More work is required to clarify the relationship between thermal advection and the ageostrophic wind. However, it appears that the synoptic-scale ascent or subsidence accompanying thermal advection may be responsible for the non-geostrophic components of the flow for the two cases studied.

5.3 Suggestions for Further Work

Perhaps this investigation would be aided most by studying several more cases of strong flow across the Western Cordillera to try and determine if there is some feature of the ageostrophic wind field which appears regularly over some portions of the terrain. In this connection, and in the light of the results of the present study,

it would be advisable to check the atmospheric soundings closely for the prevailing stabilities and the levels at which condensational heating would be most significant. Also, it would probably be of some help in identifying terrain effects if the grid were expanded to include more area east of the Cordillera. This expansion would allow comparisons to be drawn between areas of strong and weak terrain effect. The grid expansion would probably prove most profitable over the Continental United States because of the data coverage available.

It is felt that the use of time-averaged ageostrophic winds may have resulted in a loss of the detail necessary to identify terrain influences. Thus, the study of the data for specific times as opposed to time-averaged data may prove to be of some use in resolving terrain effects, although the results would be more susceptible to observational errors. It would also be interesting to use the data at specific times to examine the conditions in the ageostrophic wind fields during periods of lee cyclogenesis to see if there is some distinguishing feature which accompanies this phenomenon.

LIST OF SYMBOLS

Overbar ($\overline{\quad}$) denotes "time average"

Asterisk ($*$) denotes "actual value", excepting virtual temperature

δ denotes "uncertainty"

A	Area as measured on a constant-pressure surface
$A_{i,j}$	The value of a variable at a grid point
$A_{x,y}$	Station value of a variable interpolated from surrounding grid points
C_i	Correction applied to a grid-point variable during an objective analysis
c	Adiabatic speed of sound in air
c_p	Specific heat at constant pressure of dry air
D, Q	Respectively, the divergence and vorticity on a reference surface
D_p, Q_p	Isobaric divergence and vorticity, respectively
D_F, D_B	Isobaric divergence calculated by the fundamental and Bellamy methods, respectively
D_G, Q_G	Respectively, the isobaric divergence and vorticity of the gradient wind
d_i	Distance on the grid from the i^{th} station
f	$= 2\Omega \sin \Phi$, the Coriolis parameter
G	Gradient wind speed
g	Acceleration of gravity
H	Grid interval
h_i	Perpendicular distance from the i^{th} vertex to the opposing side of a Bellamy triangle
K	Curvature of a streamline or trajectory
L	Length scale of horizontal velocity variations
L'	Length scale of vertical velocity variations
m	Mass
N	Radius of influence used in the objective analysis
n'	Frequency of oscillation
n	Distance perpendicular to a streamline or trajectory
$O_{x,y}$	The observed station value of a variable at position (x,y) on the grid
P_x, P_y	The grid positions of an observing station in the x and y-directions, respectively
P_{px}, P_{py}	The grid positions of the principal grid point

p	Pressure
Q_F, Q_B	Isobaric relative vorticity calculated by the fundamental and Bellamy methods, respectively
R	The specific gas constant for dry air
R	Radius of curvature of a streamline or trajectory
R_E	Radius of the earth
r	The image-plane distance from the North Pole to a point on the grid measured along a meridian
S	Specific entropy
s	Distance along a streamline or trajectory
$S_{i,j}$	The grid-point value of a variable after a smoothing operation
T	Temperature ($^{\circ}\text{K}$)
T^*	$= \left(\frac{1+1.609 w}{1+w} \right) T$, the virtual temperature ($^{\circ}\text{K}$)
t	Time
U	Horizontal scale velocity
u, v	Observed wind components on an isobaric surface
u_A, v_A	Calculated ageostrophic wind components on an isobaric surface
u_g, v_g	Calculated geostrophic wind components on an isobaric surface
\vec{V}	Observed wind vector
\vec{V}_A	Ageostrophic wind vector on an isobaric surface
\vec{V}_g	Geostrophic wind vector on an isobaric surface
W_i	$= \frac{N^2 - d_i^2}{N^2 + d_i^2}$, a weight function
\bar{W}	Scale vertical velocity
w	Mixing ratio
Z	Terrain height
\bar{Z}	Geopotential height of a pressure surface
α	The direction of the ageostrophic wind component
α_s	Angle between the reference meridian and the meridian through a station
α_p	Angle between the reference meridian and the meridian through the principal-grid-point
α_i	Wind direction at the i^{th} vertex of a Bellamy triangle
β	Wind direction measured clockwise from some reference direction

β'	Isobaric coefficient of thermal expansion
β_i	Azimuth of the side opposing the i^{th} vertex of a Bellamy triangle
Δ	Finite difference
Δ	Contour spacing
θ	A measure of the temperature difference in a fluid
κ	$= \frac{R}{c_p}$, thermal diffusivity of dry air
μ	Dynamic viscosity
ν	Kinematic viscosity
ξ	Stability factor
ρ	Density
σ^2	Variance
Φ	Latitude
ϕ	Angle between the perpendicular to a contour and the x-axis
ψ	Co-latitude
ω	$= \frac{dp}{dt}$, velocity perpendicular to an isobaric surface
∇	$= \hat{i} \frac{\partial}{\partial x} + \hat{j} \frac{\partial}{\partial y} - \hat{k} \rho g \frac{\partial}{\partial p}$, the three-dimensional del-operator
∇_p	The two dimensional del-operator on a constant-pressure surface
∇_p^2	Two-dimensional Laplacian on a constant-pressure surface

REFERENCES TO LITERATURE

- Aubert, E.F., 1957: On the Release of Latent Heat as a Factor in Large Scale Atmospheric Motions. J. Meteor., 14, pp. 527-542.
- Baird, D.C., 1962: Experimentation: An Introduction to Measurement Theory and Experiment Design. Prentice-Hall, Inc., Englewood Cliffs, 198 pp.
- Batchelor, G.K., 1967: An Introduction to Fluid Dynamics. Cambridge Univ. Press, pp. 167-171.
- Bellamy, J.C., 1949: Objective Calculations of Divergence, Vertical Velocity, and Vorticity. Bull. Amer. Meteor. Soc., 30, pp. 45-49.
- Bergthorssen, P., and B.R. Döös, 1955: Numerical Weather Map Analysis. Tellus, 7, pp. 329-340.
- Berkofsky, L., 1964: The Fall-off with Height of Terrain-Induced Vertical Motions. J. Appl. Meteor., 3, pp. 410-414.
- Charette, C.O., 1971: Streamline Patterns and Terrain-Induced Vertical Velocities in the Western Cordillera. M. Sc. Thesis, Univ. of Alberta.
- Cressman, G.P., 1959: An Operational Objective Analysis System. Monthly Wea. Rev., 87, pp. 367-374.
- Danard, M.B., 1964: On the Influence of Released Latent Heat on Cyclone Development. J. Appl. Meteor., 3, pp. 27-37.
- Eddy, A., and L. Rose, 1973: A Cursory Look at the Effect of Wind Error on Kinematic Divergence. Department of Meteorology, University of Oklahoma.
- Glahn, H.R., Hollenbaugh, G.W., and D.A. Lowery, 1969: An Operationally Oriented Objective Analysis Program. U.S. Dept. of Commerce, ESSA Technical Memorandum WBTM TDL 22, 20 pp.
- Glahn, H.R., and G.W. Hollenbaugh, 1969: An Operationally Oriented Small-Scale 500-Millibar Height Analysis. U.S. Dept. of Commerce, ESSA Technical Memorandum WBTM TDL 19, 18 pp.
- Godson, W.L., 1950: A Study of the Deviations of Wind Speeds and Directions from Geostrophic Values. Quart. J. Roy. Meteor. Soc., 76, pp. 3-15.

- Haltiner, G.J., 1971: Numerical Weather Prediction. John Wiley & Sons, Inc., N.Y., 317 pp.
- Hopkinson, R.F., 1972: A Study of Orographically Induced Vertical Velocity and Precipitation in Western Canada. M.Sc. Thesis, Univ. of Alberta.
- Namias, J. and P.F. Clapp, 1946: Normal Fields of Divergence and Convergence at the 10,000-Foot Level. J. of Meteor., 3, pp. 14-22.
- Petterssen, S., 1956: Weather Analysis and Forecasting. Vol. 1, 2nd ed., McGraw-Hill Book Co., N.Y., 428 pp.
- Rapp, R.R., 1952: The Effect of Variability and Instrument Error on Measurements in the Free Atmosphere. Meteorological Papers, Vol. 2, No. 1, New York Univ. College of Engineering, 41 pp.
- Saucier, W.J., 1955: Principles of Meteorological Analysis. Univ. of Chicago Press, Chicago, p. 33.
- Sawyer, J.S., 1959: The Introduction of the Effects of Topography into Methods of Numerical Forecasting. Quart. J. Roy. Meteor. Soc., 85, pp. 31-43.

APPENDIX I

DIVERGENCE AND VORTICITY USING THE BELLAMY TRIANGLE METHOD

Consider the equation of continuity in the form:

$$-\frac{1}{\rho} \frac{d\rho}{dt} = \nabla \cdot \vec{V} \quad (\text{A.1.1})$$

as applied to a parcel of air moving on a constant pressure surface having an area on this surface of A, unit thickness, and containing mass m of air. Applying (A.1.1) to this parcel would yield:

$$-\frac{A}{m} \frac{d}{dt} \left(\frac{m}{A} \right) = \nabla_P \cdot \vec{V}$$

or

$$-\frac{1}{m} \frac{dm}{dt} + \frac{1}{A} \frac{dA}{dt} = \nabla_P \cdot \vec{V} \quad (\text{A.1.2})$$

Since mass must be conserved, (A.1.2) reduces to

$$\frac{1}{A} \frac{dA}{dt} = \nabla_P \cdot \vec{V}$$

or

$$D_P = \frac{1}{A} \frac{dA}{dt} \quad (\text{A.1.3})$$

where D_P represents the velocity divergence of the parcel as it moves along the pressure surface. Let the surface area of the parcel be represented by a triangular shape as shown in Figure A1.

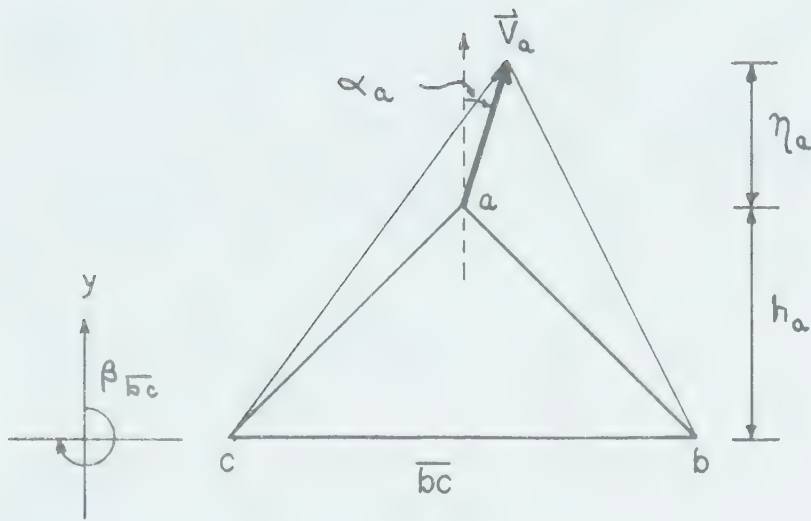


Fig. A.1 The geometry of the Bellamy Triangle.

The area of the triangle is given by

$$A = \frac{1}{2} \overline{bc} h_a$$

If we assume that the wind speed is zero at vertices b and c, and increases linearly to V_a at vertex a, then the outflow (or inflow) of air from the volume of unit thickness in some arbitrary unit time Δt is represented by

$$\Delta A = \frac{1}{2} (h_a + \eta_a) \overline{bc} - \frac{1}{2} h_a \overline{bc}$$

whence

$$D_{p_a} = \frac{1}{A} \frac{\Delta A}{\Delta t} = \frac{\eta_a}{h_a} \quad (\text{A.1.4})$$

where D_{p_a} represents the partial divergence at vertex a. Referring to Figure A1, one finds that

$$\eta_a = -V_a \sin(\beta_{bc} - \alpha_a)$$

Thus (A.1.4) can be written:

$$D_{p_a} = -\frac{V_a}{h_a} \sin(\beta_{bc} - \alpha_a)$$

Carrying through a similar argument for the remaining vertices and summing the results gives:

$$D_p = \sum_{i=1}^3 -\frac{V_i}{h_i} \sin(\beta_i - \alpha_i) \quad (\text{A.1.5})$$

where the numbers 1,2,3 are substituted for the letters a,b,c and β_i represents the azimuth of the side opposing vertex i. Results of this operation yield positive values for divergence and negative values for convergence.

To obtain the partial vertical component of vorticity at the i^{th} vertex one need only add 90° to the wind direction and use (A.1.5). Thus:

$$\begin{aligned} Q_i &= -\frac{V_i}{h_i} \sin\left(\beta_i - \left(\alpha_i + \frac{\pi}{2}\right)\right) \\ &= -\frac{V_i}{h_i} \cos(\beta_i - \alpha_i) \end{aligned}$$

and

$$Q = \sum_{i=1}^3 \frac{V_i}{h_i} \cos(\beta_i - \alpha_i) \quad (\text{A.1.6})$$

Use of (A.1.6) yields positive values for cyclonic vorticity and negative values for anticyclonic vorticity.

APPENDIX II

GRADIENT WIND VORTICITIES AND DIVERGENCES

Employing the prime notation to indicate differentiation with respect to x , the radius of curvature of a streamline (R) is given by:

$$R = \frac{(1 + y'^2)^{3/2}}{y''} \quad (\text{A.2.1})$$

Since G is assumed constant, equations (2.3.4) become:

$$D_G = G \frac{\partial \beta}{\partial n} \quad (\text{A.2.2})$$

$$Q_G = \frac{G}{R} \quad (\text{A.2.3})$$

also, since $\beta = \beta(x)$, we find:

$$\frac{\partial \beta}{\partial n} = \frac{\partial \beta}{\partial x} \frac{\partial x}{\partial n} \quad (\text{A.2.4})$$

But

$$\beta = \arctan(y') \quad (\text{A.2.5})$$

and thus:

$$\frac{\partial \beta}{\partial x} = \frac{y''}{1+y'^2} = \frac{1}{R} \sqrt{1+y'^2} \quad (\text{A.2.6})$$

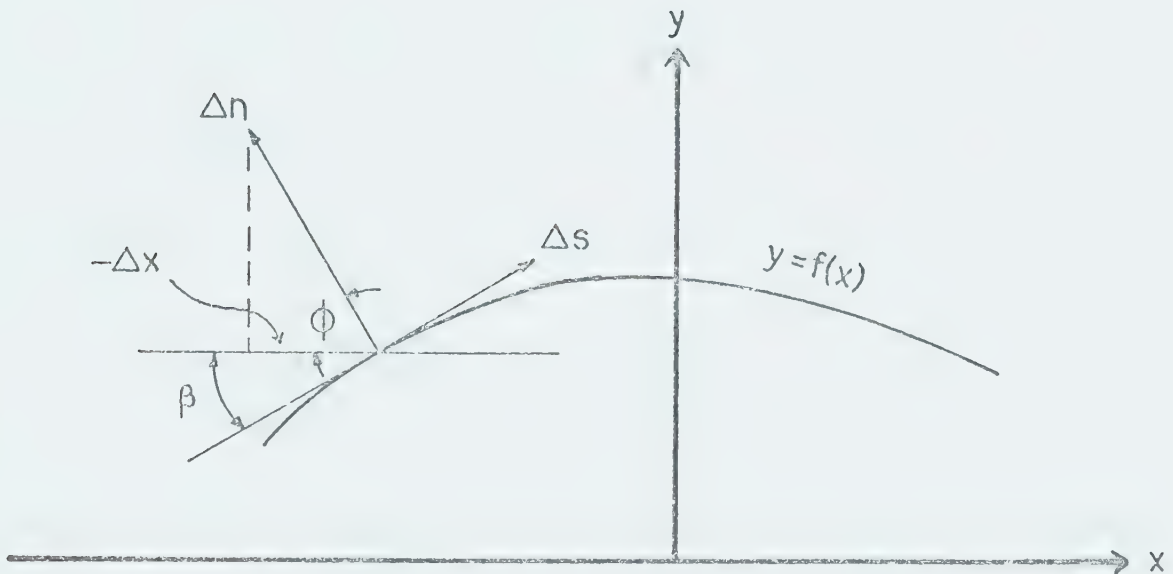


Fig. A.2 The finite-difference elements for evaluating the partial derivatives in the equations for the gradient wind divergence and relative vorticity.

Referring to Figure A.2 and using finite differences to represent the partial derivatives:

$$\frac{\partial x}{\partial n} = \frac{\Delta x}{\Delta n} = -\cos \phi \quad (\text{A.2.7})$$

but

$$\phi = \frac{\pi}{2} - \beta$$

and using (A.2.7) gives:

$$\frac{\partial x}{\partial n} = -\sin \beta \quad (\text{A.2.8})$$

Using (A.2.8) and (A.2.6) we obtain:

$$\begin{aligned} \frac{\partial \beta}{\partial n} &= -\frac{1}{R} \sqrt{1+y'^2} \sin \beta \\ &= -\frac{y'}{R} \end{aligned}$$

Thus, (A.2.2) and (A.2.3) become:

$$D_G = -\frac{G y'}{R} \quad (\text{A.2.9})$$

$$Q_G = \frac{G}{R} \quad (\text{A.2.10})$$

where R is given by (A.2.1).

Equations (A.2.9) and (A.2.10) were evaluated on an IBM 360/67 computer using $G=40 \text{ m sec}^{-1}$, and x and y were taken to be measured in grid intervals of 185.3 km. Values were calculated for $x=-10$ to 10 in increments of 0.5.

Since the parameters (i.e. R , y' , etc.) do not change if a different value of G is chosen, it is clear that:

$$D_{G'} = \left(\frac{G'}{G_0} \right) D_{40}$$

and

$$Q_{G'} = \left(\frac{G'}{G_0} \right) Q_{40}$$

where $D_{G'}$ and $Q_{G'}$ are the divergence and vorticity estimates for the new gradient wind speed G' .

APPENDIX III

DERIVATION OF THE UNCERTAINTIES IN THE DIVERGENCE AND VORTICITIES CALCULATED BY THE FUNDAMENTAL AND BELLAMY METHODS

In finite difference notation, the geostrophic wind components calculated from the height field are given by:

$$u_g = -\frac{g}{2fH} (z_2 - z_4)$$

$$v_g = \frac{g}{2fH} (z_3 - z_1)$$
(A.3.1)

where H is the grid interval, the image factor of the map has been neglected, and the subscripts refer to the points as given in Figure A.3.

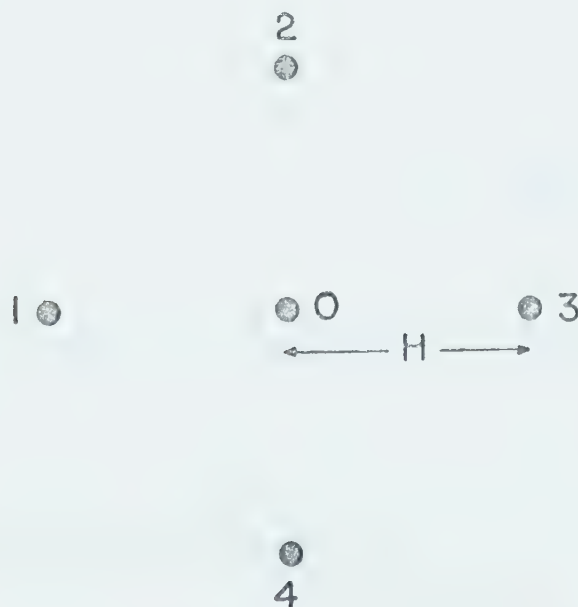


Fig. A.3 The grid-point ordering for calculating the geostrophic winds on a constant pressure surface.

In the following derivations, only the equations for the west-east component of velocity (u) will be presented where possible, since those for the north-south component (v) will have the same form.

In that the pressure heights at the grid points are just extrapolations from the data points, the uncertainties in the initial data set (i.e. the heights calculated from the radiosonde data) will be communicated to the grid point values. To try and calculate how much of the initial uncertainty in the height values will be transferred to the grid points by the objective analysis routine would be difficult. In lieu of this, it was assumed that the uncertainty (δZ) in the initial data set would apply equally to the grid values.

Using this assumption, (A.3.1) can be expressed as:

$$u_g^* = u_g \pm g \frac{\delta Z}{f H} \quad (\text{A.3.2})$$

where u_g , v_g are the calculated values, and superscript * is used to indicate "actual value".

Using (A.3.2), the ageostrophic components of the wind are:

$$u_A^* = (u - u_g) = (u \pm \delta u) - (u_g \pm g \frac{\delta Z}{f H}) \quad (\text{A.3.3})$$

where u and v are the observed wind components. Letting $u_A = u - u_g$, (A.3.3) can be written as:

$$u_A^* = u_A \pm (\delta u + g \frac{\delta Z}{f H}) \quad (\text{A.3.4})$$

The average of the ageostrophic components at a given level at a given point can thus be expressed as:

$$\overline{u}_A^* = \overline{u - u_g} \pm \frac{1}{l} \sum_{i=1}^l \left(\delta u + g \frac{\delta z}{fH} \right)_i \quad (\text{A.3.5})$$

where l is the number of values over which the average was taken. However, since δu and δz are not considered functions of time, (A.3.5) can be simplified to:

$$\begin{aligned} \overline{u}_A^* &= \overline{u - u_g} \pm \left(\delta u + g \frac{\delta z}{fH} \right) \\ &= \overline{u}_A \pm \delta \overline{u}_A \end{aligned} \quad (\text{A.3.6})$$

Employing finite differences to evaluate the derivatives gives the average fundamental divergence (\overline{D}_F^*):

$$\overline{D}_F^* \approx \overline{D}_F \pm \left\{ \frac{1}{H} (\delta u + \delta v) + 2g \frac{\delta z}{fH^2} \right\} \quad (\text{A.3.7})$$

The uncertainty involved in the fundamental vorticity would be identical. Thus:

$$\delta \overline{D}_F = \delta \overline{Q}_F = \pm \left\{ \frac{1}{H} (\delta u + \delta v) + 2g \frac{\delta z}{fH^2} \right\} \quad (\text{A.3.8})$$

where $\delta \overline{D}_F$ and $\delta \overline{Q}_F$ are the uncertainties in the average divergence and vorticity calculated by the fundamental method.

Let us now examine the Bellamy method of divergence calculation as given by (1.2.2):

$$D_B = -\frac{V}{h} \sin(\beta - \alpha) \quad (A.3.9)$$

Since the Bellamy calculations utilized the average ageostrophic components, the wind speed in (A.3.9) is given by:

$$V = \sqrt{\overline{u}_A^2 + \overline{v}_A^2} \quad (A.3.10)$$

This means that the angle α represents the direction of the average ageostrophic wind as measured in a clockwise manner from the y-axis of the grid, or:

$$\alpha = \arctan\left(\frac{\overline{u}_A}{\overline{v}_A}\right) \quad (A.3.11)$$

From calculus:

$$\delta V = \frac{\partial V}{\partial u} \delta u + \frac{\partial V}{\partial v} \delta v$$

and using (A.3.10) gives:

$$\delta V = \frac{1}{\sqrt{\overline{u}_A^2 + \overline{v}_A^2}} (\overline{u}_A \delta \overline{u}_A + \overline{v}_A \delta \overline{v}_A) \quad (A.3.12)$$

Similarly

$$\delta \alpha = \frac{\partial \alpha}{\partial u} \delta u + \frac{\partial \alpha}{\partial v} \delta v$$

and using (A.3.11) gives:

$$\delta \alpha = \frac{1}{\bar{u}_A^2 + \bar{v}_A^2} (\bar{v}_A \delta \bar{u}_A - \bar{u}_A \delta \bar{v}_A) \quad (\text{A.3.13})$$

Now, from (A.3.9)

$$\delta \bar{D}_B = - \frac{\sin(\beta - \alpha)}{h} \delta V + \frac{V}{h} \cos(\beta - \alpha) \delta \alpha \quad (\text{A.3.14})$$

Substituting for V , δV , and $\delta \alpha$ and simplifying gives:

$$\begin{aligned} \delta \bar{D}_B = & \frac{1}{h \sqrt{\bar{u}_A^2 + \bar{v}_A^2}} \left\{ \cos(\beta - \alpha) [\bar{v}_A \delta \bar{u}_A - \bar{u}_A \delta \bar{v}_A] \right. \\ & \left. - \sin(\beta - \alpha) [\bar{u}_A \delta \bar{u}_A + \bar{v}_A \delta \bar{v}_A] \right\} \end{aligned}$$

However, since (A.3.9) must be evaluated at the three vertices of the triangle and the results summed, the total uncertainty

in the Bellamy divergence becomes:

$$\delta \bar{D}_B = \pm \sum_{i=1}^3 \left[\frac{1}{h \sqrt{\bar{u}_A^2 + \bar{v}_A^2}} \left\{ \cos(\beta - \alpha) [\bar{v}_A \delta \bar{u}_A - \bar{u}_A \delta \bar{v}_A] - \sin(\beta - \alpha) [\bar{u}_A \delta \bar{u}_A + \bar{v}_A \delta \bar{v}_A] \right\} \right]_i \quad (\text{A.3.15})$$

Carrying through a similar analysis for the Bellamy vorticities gives:

$$\delta \bar{Q}_B = \pm \sum_{i=1}^3 \left[\frac{1}{h \sqrt{\bar{u}_A^2 + \bar{v}_A^2}} \left\{ \cos(\beta - \alpha) [\bar{u}_A \delta \bar{u}_A + \bar{v}_A \delta \bar{v}_A] + \sin(\beta - \alpha) [\bar{v}_A \delta \bar{u}_A - \bar{u}_A \delta \bar{v}_A] \right\} \right]_i \quad (\text{A.3.16})$$

Making the following approximations: $h \approx 3H$, $\delta u \approx \delta v$, and taking $\sin(\beta - \alpha)$, $\cos(\beta - \alpha)$ to be of order one will simplify (A.3.15) and (A.3.16) to:

$$\delta \bar{D}_B \approx \pm \frac{2}{H} \left(\frac{\bar{u}_A}{\sqrt{\bar{u}_A^2 + \bar{v}_A^2}} \right) \left(\delta u + g \frac{\delta z}{fH} \right) \quad (\text{A.3.17})$$

$$\delta \bar{Q}_B \sim \pm \frac{2}{H} \left(\frac{\bar{v}_A^2}{\sqrt{\bar{u}_A^2 + \bar{v}_A^2}} \right) \left(\delta u + g \frac{\delta Z}{fH} \right) \quad (\text{A.3.18})$$

where it has been further assumed that the terms involving \bar{u}_A and \bar{v}_A have some average value for the three vertices.

With the above assumptions (A.3.8) becomes:

$$\delta \bar{D}_F = \delta \bar{Q}_F \sim \pm \frac{2}{H} \left(\delta u + g \frac{\delta Z}{fH} \right) \quad (\text{A.3.19})$$

Using (A.3.17), (A.3.18) and (A.3.19) to evaluate the ratios $\delta \bar{D}_B / \delta \bar{D}_F$ and $\delta \bar{Q}_B / \delta \bar{Q}_F$ gives the result that the uncertainties in the Bellamy divergence will be less than that of the fundamental method if $|\bar{u}_A| > 0$, while the same result applies for the vorticities if $|\bar{v}_A| > 0$.

APPENDIX IV

THE EQUATIONS FOR TRANSFORMING GEOGRAPHICAL POSITIONS INTO GRID POSITIONS

Let the grid point (15,1) be called the principal-grid-point.
Let the grid position of the principal-grid-point be P_p .
Let the grid position of the station be P_s .
Then the grid positions for the station will be given by:

$$x_s = P_{sx} - P_{px} + 1$$

$$y_s = 15 - (P_{py} - P_{sy})$$

(A.4.1)

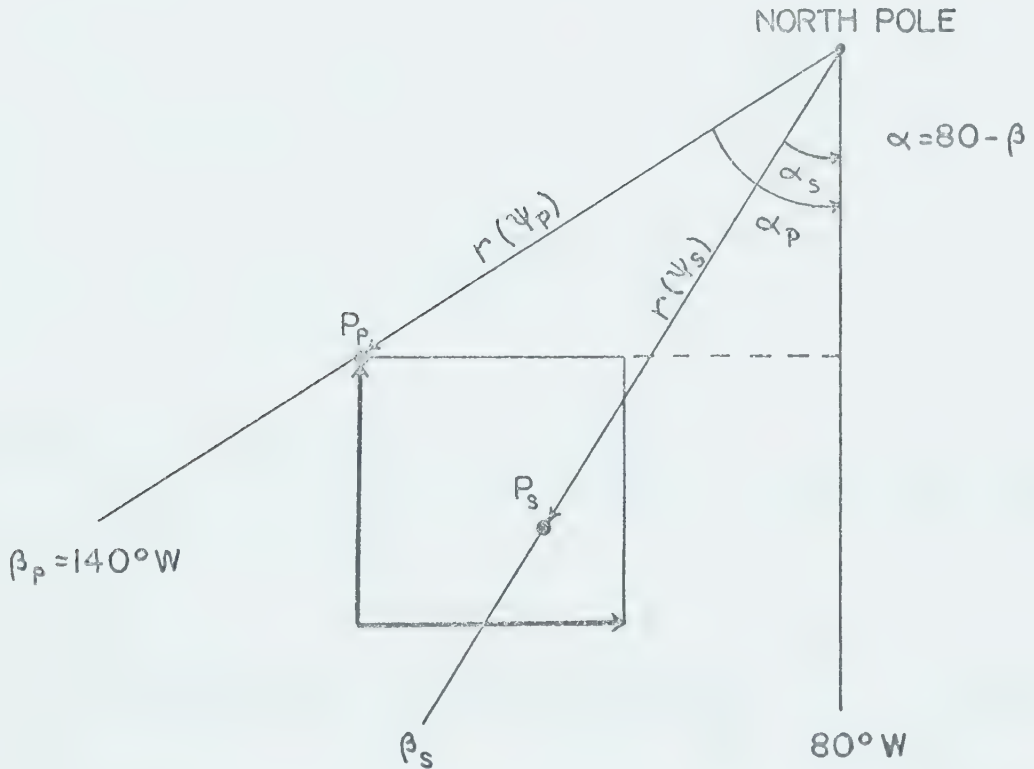


Fig. A.4 The image-plane geometry for transforming latitude and longitude into grid-point positions.

Referring to Figure A.4 one finds that:

$$P_{py} = \frac{1}{H} \{ r(\psi_R) - r(\psi_p) \cos \alpha_p \}$$

(A.4.2)

$$P_{px} = \frac{1}{H} \{ r(\psi_p) \sin \alpha_p \}$$

in which r is the distance in kilometers from the pole to the point as measured along a meridian on the image plane, ψ_R is the reference co-latitude (40°N), ψ_p is the co-latitude of the principle-grid-point (40°N).

Similarly:

$$P_{sy} = \frac{1}{H} \{ r(\psi_R) - r(\psi_s) \cos \alpha_s \}$$

(A.4.3)

$$P_{sx} = \frac{1}{H} \{ r(\psi_s) \sin \alpha_s \}$$

where ψ_s is the co-latitude of the station.

For a polar stereographic projection, Saucier (1955) gives the expression for $r(\psi)$ as:

$$r(\psi) = R_E (1 + \cos \psi_0) \tan \frac{\psi}{2}$$

(A.4.4)

in which Ψ is the co-latitude of the desired point, R_E is the radius of the earth (6371.22 km), and Ψ_0 is the standard co-latitude for the map projection (30°N). Equation (A.4.4) incorporates the image scale $m = \frac{1 + \cos \Psi_0}{1 + \cos \Psi}$.

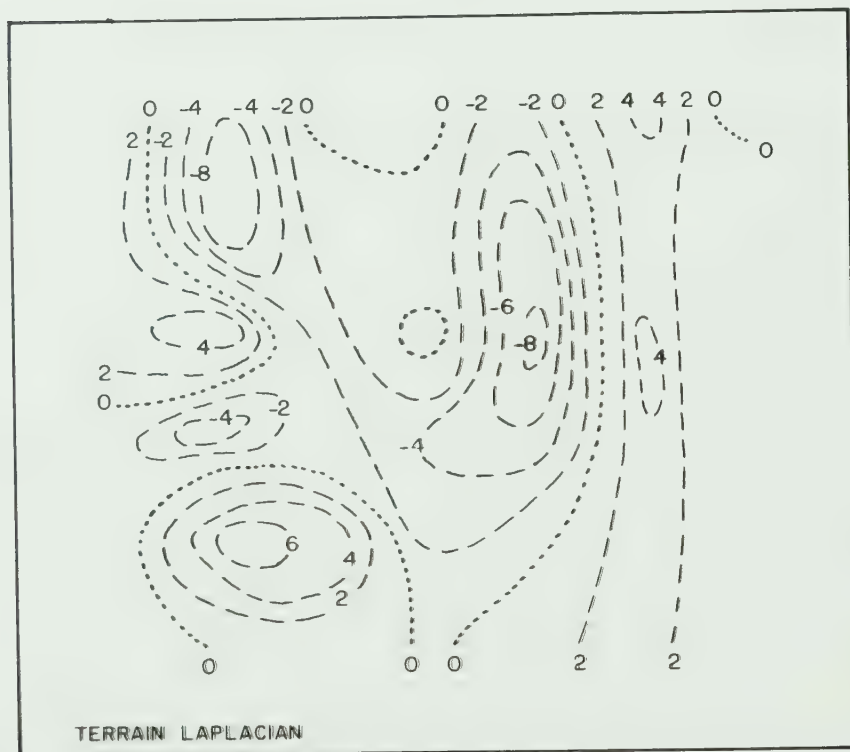
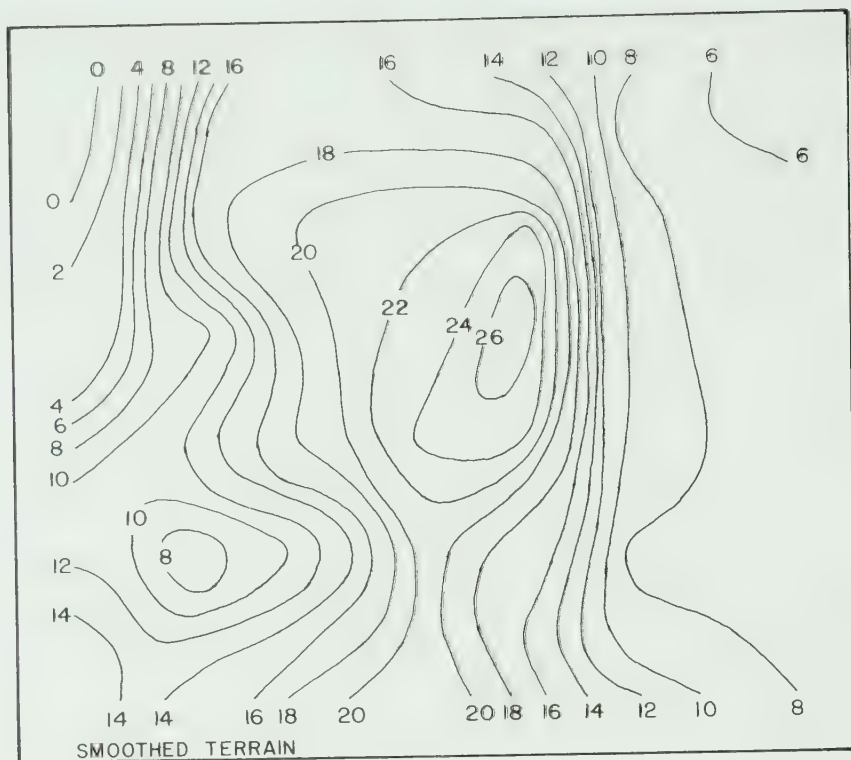
Combining (A.4.1), (A.4.2), (A.4.3) and using (A.4.4) gives:

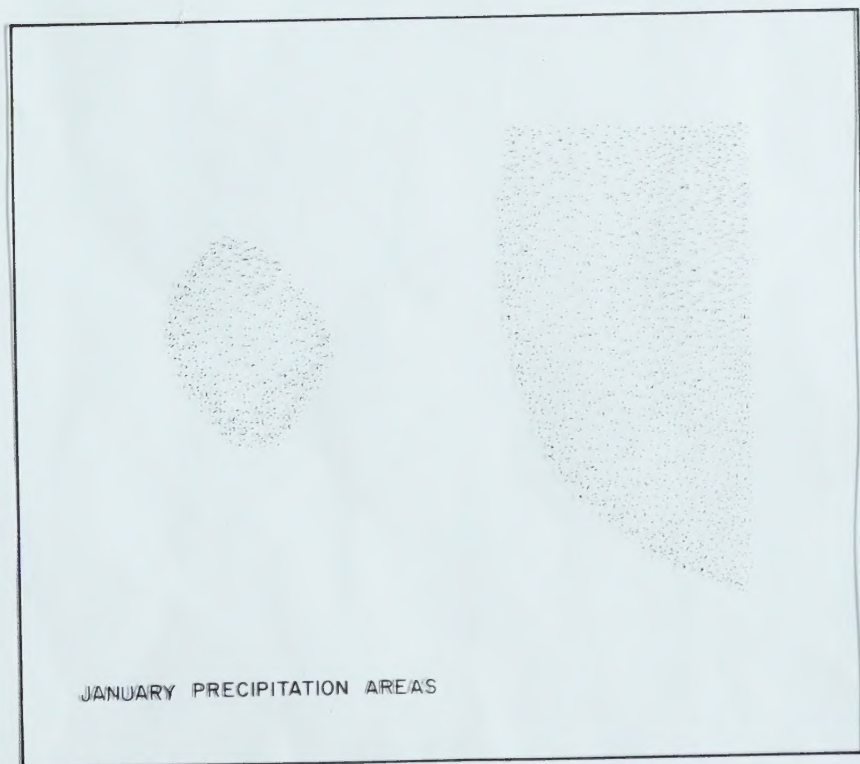
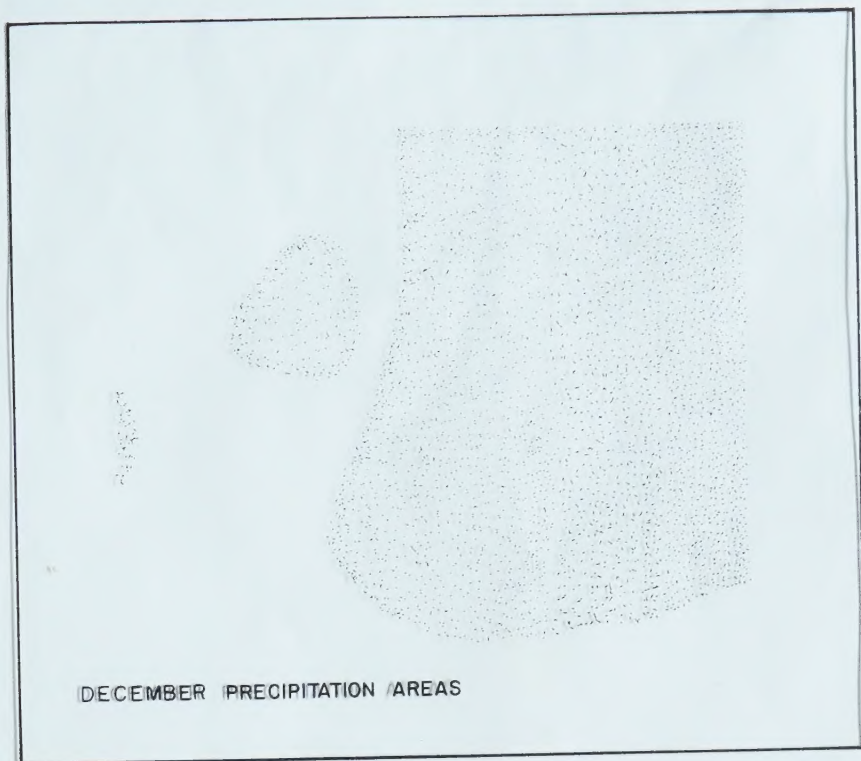
$$y_s = 15 + \frac{J}{H} \left(\tan \frac{\Psi_p}{2} \cos \alpha_p - \tan \frac{\Psi_s}{2} \cos \alpha_s \right) \quad (\text{A.4.5})$$

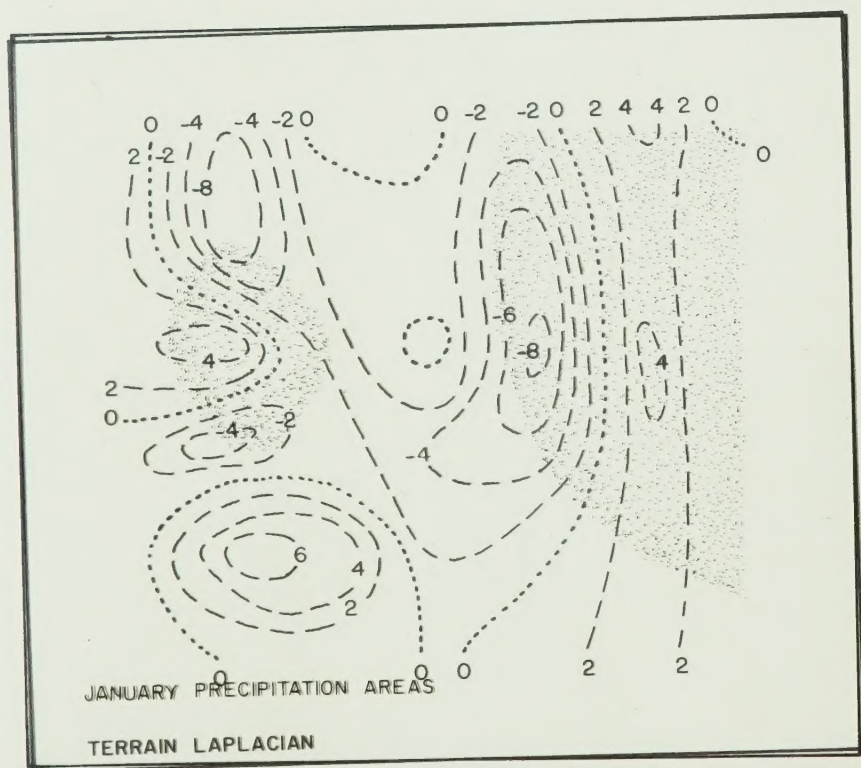
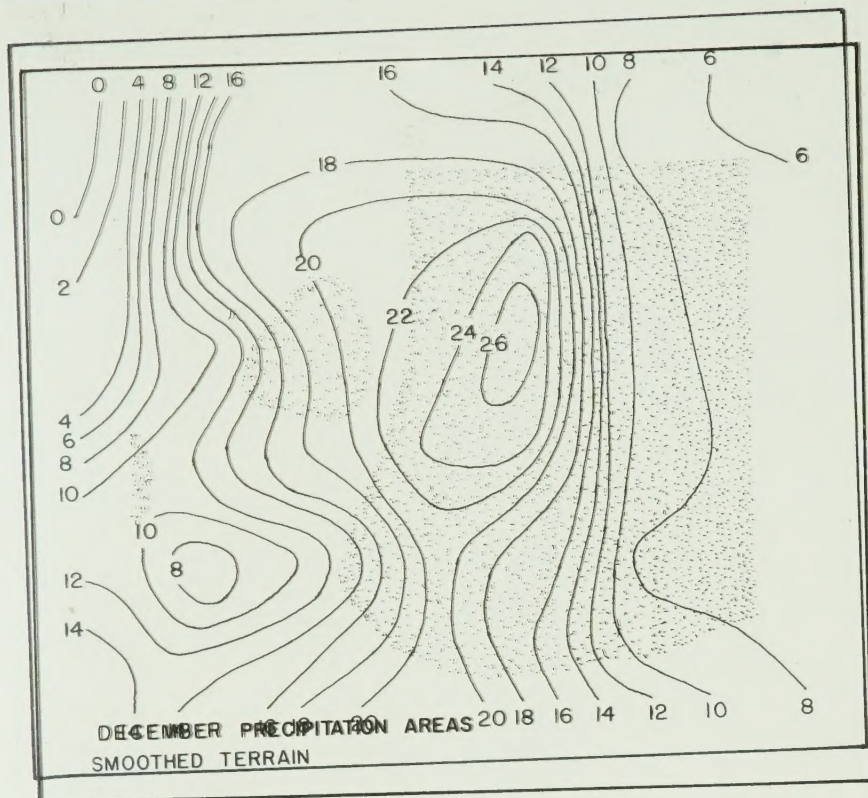
$$x_s = 1 + \frac{J}{H} \left(\tan \frac{\Psi_s}{2} \sin \alpha_s - \tan \frac{\Psi_p}{2} \sin \alpha_p \right)$$

where

$$J = R_E (1 + \cos \Psi_0)$$









B30059